Inline Coupling of Simple and Complex Chemistry Modules within the Global Weather Forecast model FIM (FIM-Chem v1)

Li Zhang[1, 2] [*], Georg A. Grell[2], Stuart A. McKeen[1,3], Ravan Ahmadov[1,2], Karl D. Froyd[1,3],

Daniel Murphy[3]

[1]*Cooperative Institute for Research in Environmental Sciences (CIRES), University of Colorado, Boulder, CO, USA*

[2]*NOAA/Global Systems Laboratory, Boulder, CO, USA*

[3]*NOAA/Chemical Sciences Laboratory, Boulder, CO, USA*

15
16
17
18
19
20
21

*Correspondence to: Li Zhang (kate.zhang@noaa.gov)

CIRES, University of Colorado Boulder

GSL EPAD, NOAA ESRL

325 Broadway David Skaggs Research Center R/GSL1

Boulder, CO 80305

1-303-497-3956

1   **Abstract.**

2   The global Flow-following finite-volume Icosahedral Model (FIM), which was developed in the Global

3   Systems Laboratory of NOAA/ESRL, has been coupled inline with aerosol and gas-phase chemistry schemes

4   of different complexity using the chemistry and aerosol packages from WRF-Chem v3.7, named as FIM-

5   Chem v1. The three chemistry schemes include 1) the simple aerosol modules from the Goddard Chemistry

6   Aerosol Radiation and Transport model that includes only simplified sulfur chemistry, bulk aerosols, and

7   sectional dust and sea salt modules (GOCART); 2) the photochemical gas-phase mechanism RACM coupled

8   to GOCART to determine the impact of more realistic gas-phase chemistry on the GOCART aerosols

9   simulations (RACM_ GOCART); and 3) a further sophistication within the aerosol modules by replacing

10   GOCART with a modal aerosol scheme that includes secondary organic aerosols (SOA) based on the VBS

11   approach (RACM_SOA_VBS). FIM-Chem is able to simulate aerosol, gas-phase chemical species and SOA

12   at various spatial resolutions with different levels of complexity and quantify the impact of aerosol on

13   numerical weather predictions (NWP). We compare the results of RACM_ GOCART and GOCART schemes

14   which uses the default climatological model fields for OH, H_2O_2, and NO_3. We find significant reductions of

15   sulfate that are on the order of 40% to 80% over the eastern US and are up to 40% near the Beijing region

16   over China when using the RACM_GOCART scheme. We also evaluate the model performance by

17   comparing with the Atmospheric Tomography Mission (ATom-1) aircraft measurements in 2016 summer.

18   FIM-Chem shows good performance in capturing the aerosol and gas-phase tracers. The model predicted

19   vertical profiles of biomass burning plumes and dust plumes off the western Africa are also reproduced

20   reasonably well.

1 Introduction

The impacts of aerosol on weather and climate are generally attributed to the direct, semidirect, indirect, and surface albedo effects, with the direct effect predominating radiative forcing over a global scale [e.g. *Bauer and Menon*, 2012]. However, there are significant differences in estimates of direct aerosol radiative forcing between various global aerosol models, particularly with respect to the attribution of forcing to specific aerosol species and sources [*Myhre et al*., 2013]. Discrepancies in direct radiative forcing are also found between global aerosol model results and determinations based on satellite retrievals, with assumptions related to aerosol composition and optical properties as the primary source of difference [*e.g. Su et al.,* 2013]. Several processes and steps are necessary to accurately include aerosol effects within a meteorological forecast. Aerosol abundance, composition, and size distribution are the basic quantities needed within calculations of the optical properties, which in turn are used within radiative transfer calculations to calculate heating or cooling rates and are incorporated within the thermodynamic calculations of the numerical forecast. The importance of aerosol impacts on the meteorological fields for climate modeling have been widely recognized by many studies [e.g. Xie et al., 2013; Yang et al., 2014; *Wang et al.*, 2014a, 2014b; Colarco et al., 2014]. Since it is increasingly common for modeling systems to start using prognostic online aerosol schemes and more accurate emissions, many studies exist that show the importance of including aerosols at least for case studies or over limited time periods. On NWP timescales (5–10 days), Rodwell and Jung [2008] showed an improvement in forecast skill and general circulation patterns in the tropics and extra-tropics by using a monthly varying aerosol climatology rather than a fixed climatology in the European Centre for Medium-Range Weather Forecasting (ECMWF) global forecasting system. The inclusion of the direct and indirect effects of aerosol complexity into a version of the global NWP configuration of the Met Office Unified Model (Met UM) shows that the prognostic aerosol schemes are better able to predict the temporal and spatial variations of atmospheric aerosol optical depth, which is particularly important in cases of large sporadic aerosol events such as large dust storms or forest fires [Mulcahy et al., 2014]. The aerosols from biomass burning sources have been shown to have an effect on large-scale weather patterns within global scale models [e.g. Sakaeda, 2011] and synoptic scale meteorology within the WRF-Chem regional model [Grell et al., 2011]. Toll et al. [2015] showed considerable improvement in forecasts of near-surface conditions during Russian wildfires in summer 2010 by including the direct radiative effect of realistic aerosol distributions. Likewise, many global models [*e.g. Haustein et al*., 2012] and regional models [*e.g.* WRF-Chem, *Zhao et al*., 2010] have established a clear connection between dust emissions and weather patterns over synoptic to seasonal time scales. While positive impacts of predicted aerosols on weather forecasts have been shown on an episodic basis, a systematic verification of current state-of-the-art operational modeling systems does not yet demonstrate that the impact is statistically significant over longer periods of time to warrant the required additional computational resources [Peuch et al., 2014]. Operational forecast systems are usually highly tuned and still use aerosol climatologies. The inclusion of aerosols in the presence of strong sources or sinks should lead to an improvement of predictive skills. A successful example of a short-range weather forecasting coupled with the smoke tracer is the High-Resolution Rapid Refresh

coupled with Smoke (HRRR-Smoke) model [Ahmadov et al, 2017]. The model forecasts 3D smoke concentrations and its radiative impacts over the CONUS domain at 3km spatial gridding [https://rapidrefresh.noaa.gov/hrrr/HRRRsmoke/].

By applying the chemistry package from WRF-Chem v3.7 into the Flow-following finite-volume Icosahedra Model (FIM, Bleck et al. 2015), named as FIM-Chem v1, we essentially make it possible to explore the importance of different levels of complexity in gas and aerosol chemistry, as well as in physics parameterizations on the interaction processes in global modeling systems. FIM is used in the sub-seasonal experiment (SUBx) for sub-seasonal to seasonal (S2S) forecasting and is now considered a steppingstone towards NOAA's Next Generation Global Prediction System, which will be based on the third generation non-hydrostatic Finite Volume Cubed Sphere (FV3) dynamic core [Sun et al., 2018a, b]. The chemistry component created here is designed to be moved flawlessly into FV3. WRF-Chem currently has 63 different gas and aerosol chemistry options, as well as several microphysics and radiation parameterizations, which are coupled to chemistry to simulate direct and indirect aerosol feedback processes. In this study we demonstrate three examples of different complexities on the aerosol forecasts by FIM-Chem. The current real-time forecast uses simple bulk aerosol modules from the GOCART model, with a simplified chemistry for sulfate production. This chemistry scheme does not include NOx/VOC gas chemistry or SOA formation. Currently the real-time GOCART application uses climatological fields of OH, H_2O_2 and NO_3 to drive the oxidation of SO_2 and oceanic dimethyl sulfide to sulfate.

Here we also investigate the sensitivity to the addition of complex gas-phase chemistry and a more reasonable inclusion of Secondary Organic Aerosol formation. Organic matter makes up the significant fraction of the sub-micron aerosol composition [*Zhang et al.*, 2007], and organic aerosol (OA) along with sulfate and black carbon are believed to be the main anthropogenic contributors to direct radiative forcing on a global scale [*Myhre et al*., 2013]. A computationally efficient SOA parameterization based on the Volatility Basis Set approach [Donahue, 2011] was implemented in WRF-Chem by Ahmadov et al. (2012).

To evaluate the model performance, the observation data from the NASA Atmospheric Tomography aircraft mission (ATom-1, 2016) is used, in which the DC-8 is instrumented to make high-frequency in situ measurements of the most the chemical species over the Pacific and Atlantic Oceans, and across the Arctic and US, to evaluate the model performance. Section 2 describes some aspects of the FIM and FIM-Chem model, the coupling of aerosol configurations, gas-phase chemical schemes and an overview of the observation data used to evaluate the model results. The chemical weather forecasts by using three different gas and aerosol chemistry schemes with different level of complexities are shown in Section 3. Section 4 presents the evaluations of the chemical weather forecasts, and the model evaluations are investigated in Section 5. We end with discussion and conclusions in Section 6.

2 Models and Observation

2.1 FIM

1 FIM is a hydrostatic global weather prediction model based on an icosahedral horizontal grid and a hybrid
2 terrain following/isentropic vertical coordinate [Bleck et al., 2015]. Icosahedral grids are generated by
3 projecting an icosahedron onto its enclosing sphere and iteratively subdividing the 20 resulting spherical
4 triangles until a desired spatial resolution is reached. The main attraction of geodesic grids lies in their fairly
5 uniform spatial resolution and in the absence of the two pole singularities found in spherical coordinates. The
6 primary purpose of using a near-isentropic vertical coordinate in a circulation model is to assure that
7 momentum and mass field constituents (potential temperature, moisture, chemical compounds, etc.) are
8 dispersed in the model in a manner emulating reality, namely, along neutrally buoyant surfaces. The FIM
9 model has been tested extensively on real-time medium-range forecasts to ready it for possible inclusion in
10 operational multi-model ensembles for medium-range to seasonal prediction, and the following simulations
11 are performed at G6 (~128 km) horizontal resolution.

12 In FIM-Chem, the column physics parameterizations have been taken directly from the 2011 version of the
13 GFS [Bleck et al., 2015]. The physical parameterizations include the Grell-Freitas convection
14 parameterization [Grell and Freitas, 2014], the Lin et al. [1983] cloud microphysics scheme, coupled to the
15 model aerosol parameterization and modified to include second moment effects, and the land surface
16 processes simulated by the NCEP's Noah land surface model [Koren et al. 1999 and Ek et al. 2003].

17 **2.2 FIM-Chem**

18 FIM-Chem, is a version of the FIM model coupled inline with chemical transport model including three
19 aerosol and gas-phase chemistry schemes of different complexities, where physics and chemistry components
20 of the model are simulated simultaneously. The chemical modules and coupling schemes are adopted from
21 the WRF-Chem model v3.6.1 [Grell et al. 2005; Fast et al. 2006; Powers et al., 2017].

22 **2.2.1 GOCART scheme**

23 The first chemical option is the simplest aerosol modules that from the GOCART model, which includes
24 simplified sulfur chemistry for sulfate simulation from chemical reactions of SO_2, H_2O_2, OH, NO_3 and DMS,
25 bulk aerosols of black carbon (BC), organic carbon (OC), and sectional dust and sea salt. For OC and BC,
26 hydrophobic and hydrophilic components are considered and the chemical reactions using prescribed OH,
27 H_2O_2, and NO_3 fields for gaseous sulfur oxidations [*Chin et al.*, 2000]. The dust scheme is using the Air
28 Force Weather Agency (AFWA) scheme with five dust size bins [LeGrand et al., 2019]. The bulk vertical
29 dust flux is based on the Marticorena and Bergametti scheme [Marticorena et al., 1995], whereas the particle
30 size distribution is built according to Kok, 2011, which is based on the brittle material fragmentation theory.
31 Four size bins are considered for the sea salt simulation. The sea salt emissions from the ocean are highly
32 dependent on the surface wind speed [Chin et al., 2000].

33 **2.2.2 RACM_ GOCART scheme**

1   Based on the GOCART aerosol module, the second chemical option includes the photochemical gas-phase
2   mechanism of Regional Atmospheric Chemistry Mechanism (RACM), which is able to determine the impact
3   of the additional gas-phase complexity on the aerosol simulations (RACM_GOCART). The RACM
4   chemistry mechanism is based upon the earlier Regional Acid Deposition Model, version 2 (RADM2)
5   mechanism [Stockwell t al., 1990] and the more detailed Euro-RADM mechanism [Stockwell and Kley,
6   1994]. It includes a full range of photolysis, biogenic VOCs, full NOx/VOC chemistry, inorganic and organic
7   gaseous species to perform air pollution studies that includes rate constants and product yields from the most
8   laboratory measurements [Stockwell et al., 1997]. The simplified sulfur chemistry for sulfate formation does
9   not use climatological fields of OH, H_2O_2 and NO_3 from GOCART model to drive the oxidation of SO_2 as
10 that in GOCART, and it is replaced by explicitly simulating the gas-phase RACM chemistry.

11 **2.2.3 RACM_SOA_VBS scheme**

12 The simple GOCART scheme does not include photolysis, full gas chemistry and secondary organic aerosol
13 production, and it normally uses climatological fields of OH, H_2O_2 and NO_3 to drive the oxidation of
14 SO_2 and oceanic dimethyl sulfide (DMS) to produce sulfate. We implemented a more complex gas-aerosol
15 chemistry scheme in FIM-Chem. This scheme includes RACM based gas chemistry and updated SOA
16 scheme, which is based on the VBS approach [Ahmadov et al., 2012]. The RACM_SOA_VBS scheme
17 includes photolysis reactions for multiple species, full nitrogen and VOC (anthropogenic and biogenic)
18 chemistry, inorganic and organic aerosols. All the secondary gas species that are required for the SO_2
19 oxidation are simulated explicitly by the gas chemistry scheme here.

20 **2.3.4 Emission, deposition, and aerosol optical properties**

21 The preprocessor PREP-CHEM-SRC v1.5 [Freitas et al., 2011], a comprehensive tool aiming at preparing
22 emission fields of the chemical species for use in atmospheric-chemistry transport models, is used to generate
23 the emissions for FIM-Chem. It includes the HTAP v2 global anthropogenic emission inventory [Janssens-
24 Maenhout et al., 2015] and biogenic VOC emissions simulated by the of Emissions of Gases and Aerosols
25 from Nature (MEGAN) v2.0 parameterization [Guenther et al., 2006]. The diurnal variability based on a
26 function of anthropogenic activities is applied to the HTAP emissions and the diurnal cycle of solar radiation
27 and air temperature is applied to the biogenic emissions. The biomass burning emission estimated by the
28 Brazilian Biomass Burning Emissions Model [3BEM, Longo et al. 2010; Grell et al., 2011) is also included
29 in the PREP-CHEM-SRC. The 3BEM is based on near real-time remote sensing fire products to determine
30 fire emissions and plume rise characteristics [Freitas et al., 2005, 2007; Longo et al., 2010]. The fire emissions
31 are updated as they become available and are spatially and temporally distributed according to the fire count
32 locations obtained by remote sensing of Moderate Resolution Imaging Spectroradiometer (MODIS) onboard
33 Terra and Aqua satellites [Giglio et al., 2003]. The biomass burning emission factors are from Andreae and
34 Merlot [2001]. Over the CONUS domain the MODIS data are replaced by the Wildfire Automated Biomass
35 Algorithm (WF_ABBA) processing system. The WF_ABBA is able to detect and characterize fires in near

1   real-time, providing users with high temporal and spatial resolution fire detection data

2   (http://www.ssd.noaa.gov/PS/FIRE/Layers/ABBA/abba.html). A one-dimension (1-D) time-dependent

3   cloud model implemented to calculate injection heights and emission rates online in all of the three chemical

4   schemes [Freitas et al., 2007].

5   Similar to WRF-Chem model, the flux of gases and aerosols from the atmosphere to the surface is calculated

6   by multiplying concentrations of the chemical species in the lowest model layer by the spatially and

7   temporally varying deposition velocities, the inverse of which is proportional to the sum of three

8   characteristic resistances (aerodynamic resistance, sublayer resistance, surface resistance [Grell et al. 2005].

9   The GOCART aerosol dry deposition includes sedimentation (gravitational settling) as a function of particle

10 size and air viscosity and surface deposition as a function of surface type and meteorological conditions

11 [Wesely, 1989]. The dry deposition of sulfate is described differently. In the case of simulations without

12 calculating aerosols explicitly, sulfate is assumed to be presented in the form of aerosol particles, and the dry

13 deposition of aerosol and gas phase species is parameterized as described in Erisman et al. [1994]. For

14 RACM_SOA_VBS chemical option, the dry deposition velocity of the organic condensable vapors (OCVs)

15 is parameterized as proportional to the model calculated deposition velocity of a very soluble gas, nitric acid

16 (HNO_3). The parameter which determines the fraction (denoted as "depo_fact") of HNO_3 is assumed in the

17 model since no observation constraints are available. The dry deposition velocity of HNO_3 is calculated by

18 the model during runtime [Ahmadov et al., 2012]. Wet deposition accounts for the scavenging of aerosols in

19 convective updrafts and rainout/washout in large-scale precipitation [Giorgi and Chameides, 1986; Balkanski

20 et al., 1993].

21 The aerosol optical properties such as extinction, single-scattering albedo, and the asymmetry factor for

22 scattering are computed as a function of wavelength. Each chemical constituent of the aerosol is associated

23 with a complex index of refraction. A detailed description of the computation of aerosol optical properties

24 can be found in Fast et al. [2006] and Barnard et al. [2010].

25 **2.3 Observations**

26 The Atmospheric Tomography Mission (ATom) studies the impact of human-produced air pollution on

27 greenhouse gases and on chemically reactive gases in the atmosphere [Wofsy et al., 2018]. ATom deploys

28 instrumentation to sample the atmospheric composition, profiling the atmosphere in 0.2 to 12 km altitude

29 range. Flights took place in each of 4 seasons over a 22-month period. They originated from the Armstrong

30 Flight Research Center in Palmdale, California, flew north to the western Arctic, south to the South Pacific,

31 east to the Atlantic, north to Greenland, and returned to California across central North America over the

32 Pacific and Atlantic oceans from ∼ 80°N to ∼ 65°S. ATom establishes a single, contiguous global-scale data

33 set. This comprehensive data set is used to improve the representation of chemically reactive gases and short-

34 lived climate forcers in global models of atmospheric chemistry and climate. Comparisons of model forecasts

35 with 5 flights from the first ATom mission (August 15–23, 2016) are shown here as examples of model

1 performance for specific events, such as wildfires and dust-storms, or specific conditions such as oceanic

2 versus continental.

3 The Particle Analysis by Laser Mass Spectrometry (PALMS) instrument samples the composition of single

4 particles in the atmosphere with diameters within ~150 nm - 5 μm range. It measures nearly all components

5 of aerosols from volatiles to refractory elements, including sulfates, nitrates, carbonaceous material, sea salt,

6 and mineral dust [Murphy et al., 2006]. The PALMS instrument was originally constructed for high-altitude

7 sampling [Thomson et al., 2000; Murphy et al., 2014] and has since been improved and converted for other

8 research aircraft. In August 2016, PALMS was sampling on the NASA DC-8 aircraft as part of the ATom

9 program (https://espo.nasa.gov/missions/atom/content/ATom). Aerosol composition determinations using

10 the PALMS instrument during ATom have been described and interpreted previously [Murphy et al., 2018,

11 2019; Schill et al., 2020; Bourgeois et al., 2020]. The PALMS mass concentrations for various species are

12 derived by normalizing the fractions of particles of each size and type to size distributions measured by

13 optical particle counters [Froyd et al., 2019].

14 Figure 1 shows the vertical profiles and transect time series of the ATom-1 flight tracks on August 15th and

15 17th, 2016 over Atlantic Ocean on August 23rd, 2006 over US. The August 15th flight originates from the

16 southwestern Atlantic and ends near the southern equatorial Atlantic; the August 17th flight is from the

17 southern equatorial Atlantic to the northern Atlantic; and the August 23rd flight is from Minnesota to Southern

18 California. For analysis and model validations, here we mark 16 vertical tracks and 3 horizontal tracks for

19 August 15th, 16 vertical tracks and 2 horizontal tracks for August 17th, and 8 vertical tracks and 4 horizontal

20 tracks for August 23rd.

21 **3 Chemical Composition Forecast**

22 There is a two-week spin-up period from July 15th to July 28th, since we don't use chemical initial conditions

23 at the start of the simulation time period. To provide realistic chemical initial conditions, the near real-time

24 chemical composition daily forecast has been performed from 00Z July 15th, 2016 initialized by the GFS

25 meteorological fields every 24 hours. Chemical species are cycled every 24 hours from the last output except

26 the stratospheric O_3 above tropopause which are from satellite derived fields available within GFS. O_3 It

27 should be noted that stratospheric chemistry is incomplete (no halogen chemistry) in the model, and the

28 model doesn't include any chemical data assimilation.

29 For the aerosol forecast, the GOCART and RACM_GOCART scheme are quite similar since they are using

30 the same GOCART aerosol module. However, the major difference is the impact of including gas-phase

31 chemistry on aerosol. The simpler GOCART package uses climatological fields for OH, H_2O_2, and NO_3 from

32 previous GEOS model simulations, while these species are explicitly simulated in the RACM_GOCART

33 chemistry mechanism. The PM2.5 concentrations are the sum of BC, OC, sulfate, the fine bins (diameter <

34 2.5 micrometers) of dust and sea salt. The forecast aerosol results of $PM_{2.5}$ and sulfate using GOGART and

35 RACM_GOCART and their differences (RACM_GOCART minus GOCART) are showed at Fig. 2. The

36 general patterns of $PM_{2.5}$ are quite similar in these two schemes, with the maximum surface concentrations

1   of more than 100 µg over the dust source region of western Africa, wide areas of southern Africa and polluted

2   areas of south Asia and eastern China. However, the surface concentrations of $PM_{2.5}$ in GOCART and

3   RACM_GOCART (the latter minus former) show substantial differences, decreasing more than 15 µg/m³

4   over eastern US and 20 µg/m³ over eastern China, when using the RACM_GOCART scheme. The main

5   factor that contributes to the significant differences of $PM_{2.5}$ concentration is sulfate (figures not shown here).

6   The maximum sulfate concentrations are over the eastern US, India and eastern China. We find the reductions

7   of sulfate are about 10 µg/m³ on the order of 40-80% over the eastern US and are up to 40% over eastern

8   China in RACM_GOCART (Fig. 2b). The major differences for sulfate production in the simulations is due

9   to differences in the H_2O_2, OH, and NO_3 fields. Fig. 3 shows the comparisons of H_2O_2, OH, and NO_3 between

10   GOCART and RACM_GOCART schemes. Globally the prescribed H_2O_2 in GOCART is generally larger

11   than that explicitly simulated by RACM_GOCART. The maximum of H_2O_2 regions over Africa, India and

12   eastern Asia show significant diversity. The explicitly real-simulated instantaneous H_2O_2 in RACM_

13   GOCART is much lower, by 40-60% over India and eastern Asia and 20% over eastern US, while much

14   higher (> 80%) over middle Africa, northeastern regions of Canada, and northwestern areas of South America.

15   Even though the patterns of OH are quite comparable in the GOCART and RACM_GOCART schemes, the

16   real-simulated instantaneous OH is 80% lower over eastern China when using the RACM_GOCART scheme.

17   The other big difference is over the western US with the simulated OH in RACM_GOCART being much

18   higher over northwestern US and lower over the southwestern US. The NO_3 differences are mainly over the

19   Africa and north Indian Ocean, that the real-simulated instantaneous NO_3 is much larger using the

20   RACM_GOCART scheme. Since H_2O_2 and OH are the major species converting SO_2 to sulfate, their

21   decreases cause sulfate reductions over broad areas.

22   The RACM_GOCART model is able to predict gas phase species by using the RACM gas-phase mechanism.

23   Ozone (O_3) and other gas pollutants are determined by the emissions of nitrogen oxides and reactive organic

24   species, gas- and aqueous-phase chemical reaction rates, depositions, and meteorological conditions. Fig. 4

25   represents the 120-hour surface O_3 forecast globally at 12z August 2nd and 00z August 3rd, 2016. The general

26   spatial distributions are comparable to the satellite observation. However, similar to other studies, a lot of

27   chemical transport models (CTMs) tend to significantly overestimate surface O_3 in the southeast US [Lin et

28   al., 2008; Fiore et al., 2009; Reidmiller et al., 2009; Brown-Steiner et al., 2015; Canty et al., 2015; Travis et

29   al., 2016], which is an important issue for the design of pollution control strategies [McDonald-Buller et al.,

30   2011]. We see similar problem in FIM-Chem that the predicted surface O_3 concentration on 00z August 3rd

31   2016 is also overestimated (see Fig. 4b). It well known that the O_3 production involves complex chemistry

32   driven by emissions of anthropogenic nitrogen oxide radicals (NO_x=NO+NO_2) and isoprene from biogenic

33   emissions. The primary basis of O_3 may be due to the inventory of HTAP v2 anthropogenic emission over

34   North America, which is from U.S. EPA's 2005 National Emission Inventory (NEI2005). A few studies have

35   pointed out that the NO_x emissions in the NEI-2005 and NEI-2011 from the EPA is too high [Brioude, 2011;

36   Travis et al., 2016] over the US. It must be reduced by 30-60% from mobile and industrial sources in the NEI

37   2011 inventory [Katherine et al., 2016], while the NO_x emissions over United States should be reduced more

1   for 2016 simulation since the NEI2005 NO_x emission is much larger than that of NEI2011

2   (https://cfpub.epa.gov/roe/). Also, the dry depositions of ozone, isoprene emissions and in the loss of NO_x

3   from formation of isoprene nitrates could also result into these overestimations [Lin et al., 2008; Fiore et al.,

4   2005].

5   A new SOA parameterization based on the volatility basis and VBS approach has been implemented into

6   FIM-Chem. Thus, it has the ability to simulate and predict SOA using the RACM_SOA_VBS scheme

7   [Ahmadov et al., 2012], which include the anthropogenic secondary organic aerosols (ASOA) and biogenic

8   secondary organic aerosols (BSAO) for both the nucleation and accumulation modes. Fig. 5 shows the

9   predicted SOA at 12z August 2nd and 00z August 3rd, 2016. The maximum surface SOA concentrations are

10   over the southern Africa, which may be caused by the wildfire emissions. The Eastern US, western Europe

11   and eastern Asia are the other high SOA concentrations areas. There is not significant diurnal variability for

12   the SOA spatial distributions, and the diurnal cycle of fire emission has not been included.

4 Using ATom-1 observations to evaluate the FIM-Chem Model

14   In this section, we compare 24 hours forecasts of FIM-Chem for the major aerosols and gas tracers for the

15   three different chemical schemes listed above. The FIM-Chem model results are sampled at the grid with

16   nearest latitude and longitude, and interpolated logarithmically in altitude according to the ATom-1

17   measurements. Temporally, 1-second measurements are matched to the nearest hour of the FIM-Chem hourly

18   model output, which translates into a spatial uncertainty of ~ 128 km, or ~1 model grid cell, for typical DC-

19   8 airspeeds.

4.1 Comparisons of the gas and aerosols species between FIM-Chem and the ATom-1 measurements over Atlantic

22   The comparison of some of the chemical species, e.g., EC, CO and O_3, that are mainly affected by the biomass

23   burning emissions from wild fires during August 15th and August 17th are shown in Fig. 6. The model shows

24   very good performance in reproducing the profiles of EC and CO, especially capturing the biomass burning

25   plumes near the tropics. But it also shows some differences for EC in the results of GOCART (figures not

26   shown here since it is almost the same as that of RACM_GOCART) and RACM_GOCART schemes above

27   4~5 km, where model results are overestimated. After investigating, we noticed that in the GOCART and

28   RACM_GOCART aerosol module, they both assume there is no wet deposition for externally-mixed,

29   hydrophobic BC, only for hydrophilic BC. This assumption would result into the overestimation of EC at

30   higher levels due to less wash out of hydrophobic BC. Other models with simple wet removal schemes have

31   shown similar overestimation of EC in the upper troposphere (Schwarz et al., 2013; Yu et al., 2019). However,

32   aerosols in the RACM_SOA_VBS scheme are internally mixed, so there is a much larger wet deposition,

33   and less EC in the upper levels. This an important difference about the carbonaceous aerosol for both

34   hydrophobic BC and OC in the wet removal. The comparison with the observations provides a good resource

1 for further improvements within the wet removal parameterization. The second column in Fig. 6 compares

2 CO for the observations, RACM_GOCART and RACM_SOA_VBS schemes. Overall, the forecast is able

3 to capture the observed latitude-height profiles of CO mixing ratio very well. They both show high

4 concentrations near the low altitude, though there are still some differences at the altitude that the CO mixing

5 ratio above 6 km is underestimated over the tropics while overestimated near the surface. It looks like that

6 the model does not reproduce the injection height correctly for the biomass burning emission over this area,

7 which may be due to relative weak convection or lower injection heights in the model. For O_3, the model is

8 able to consistently capture O_3 mixing ratios with both RACM_GOCART and RACM_SOA_VBS schemes,

9 including the stratospheric intrusion near 40°S at about 9 km height, though it is slightly higher near 40°N at

10 about 12 km height. We find that over equatorial areas at about 2-4 km height, the modeled O_3 mixing ratio

11 is underestimated by about 30%. This may also relate to the injection height of biomass burning that resulted

12 into much lower CO at this altitude, since CO is one of the important precursors for O_3 production. Besides

13 the aerosol and gas tracers associated with the biomass burning emissions, we also compare the HCHO, OH

14 and H_2O_2, which are the important precursors or oxidants to many other species within the RACM_GOCART

15 and RACM_SOA_VBS schemes (see Fig. 7). Generally, the pattern of the modeled HCHO mixing ratio is

16 almost the same as that of the ATom-1 measurements. The variations from south to north are captured by

17 these two schemes except a little underestimation near about 10 km height. For OH, the model reproduces

18 the vertical and temporal variations, including the large mixing ratios over the northern hemisphere. Some

19 slight differences are apparent, e.g., the overestimates over 44°S at 3-9 km height and the underestimates

20 over 40°N above 10 km height. Similarly, there is more spatial variability in the ATom-1 measurement of

21 H_2O_2. Above 6km the model overestimates H_2O_2 south of 40°S and overestimates from 20°S to the northern

22 hemisphere above 6 km. Overall, the model and ATom-1 measurement are more consistent at lower altitudes

23 for H_2O_2.

24 Figures 8 and 9 show more detailed comparisons for vertical tracks of meteorological fields and chemical

25 species in the biomass burning and dust events. For the biomass burning plume the 16th vertical profile on

26 August 15th, 2016 near 20°S is shown while the 10th profile on August 17th, 2016 near 25°N for the Saharan

27 dust plume is shown. The comparison of the meteorological fields of temperature, virtual potential

28 temperature, water vapor, relative humidity, wind speed and wind direction are shown in Fig. 8 and do not

29 change between the different chemical options. The model forecasted temperature and virtual potential

30 temperature almost overlap the ATom-1 measurements for both the August 15th and 17th vertical tracks. For

31 water vapor and relative humidity, the variations of the vertical profiles are also reproduced by the model,

32 except there are some smaller peaks in the observed profiles. There are still some differences between model

33 and ATom-1 observations for wind speed and wind direction, which may be due to model vertical resolution.

34 Overall, the model is able to capture the general vertical variations. For the chemical species (see Fig. 9),

35 the modeled EC using GOCART scheme is almost identical to that by the RACM_GOCART scheme (the

36 green line is overlapped by the blue line). Both EC concentration plots show a vertical variation of decreasing

37 with altitude and the concentrations are overestimated above 2 km in biomass burning plume (see Fig. 9a)

and above 4 km in dust storm (see Fig. 9b). The results using the RACM_SOA_VBS scheme shows much better performance to capture the vertical variations of EC. Other than a slight overestimation at 2-4 km biomass plume (see Fig. 9a first column), the EC vertical profile is very consistent to that of the observation when using RACM_SOA_VBS scheme. In the biomass burning event (see Fig. 9b first column), the modeled vertical profile with the RACM_SOA_VBS scheme captures the general changes of the vertical variations much better than those of the GOCART and RACM_GOCART schemes. As mentioned, previously, the assumption of no wet deposition for hydrophobic BC is the main reason resulting in less EC at high altitude in the RACM_SOA_VBS scheme compared to the GOCART and RACM_GOCART schemes. Due to less available observed data for sea salt, it is difficult to perform specific comparisons, but both the observation and model show strong decreases with altitude. During the dust event (see Fig. 9b third column), even though the modeled dust concentrations are lower at about 2-6 km than the observed concentrations, they are close to the observation at the surface and upper levels. For the gas-phase species, the model results are from GOCART_RACM (blue line) and RACM_SOA_VBS (red line) schemes. The observed O_3 in the biomass burning event (see Fig. 9a fourth column) shows a peak at about 2 km height, then it decreases with altitude, but increases again at about 5-9 km height. The model results from these two schemes are quite consistent. They both indicate a slight enhancement at 1.5 km height, though it is not able to capture the magnitude of the observed peak, which is underestimated by ~50%. For CO, the model can reproduce the peak at about 2 km height very well, though it overestimates the mixing ratio by 25% below 1 km in the biomass burning event (see Fig. 9a 5th column). The detailed variations of the O_3 and CO vertical profiles still show some slight differences between the model and observation, but the model generally forecasts the vertical changes with altitude, and the CO using RACM_GOCART is slightly lower than that of the RACM_SOA_VBS scheme above 5 km height.

4.2 Comparisons of aerosols and gas tracers between FIM-Chem and ATom-1 over the United States

Figure 10 shows the comparisons of EC and sulfate between ATOM-1 measurements and FIM-Chem model with three different chemical schemes over the United States. Other than the underestimates of wet removal for EC in GOCART and RACM_GOCART schemes that result in the overpredicted EC concentrations above 4 km height, the near surface (below 4 km) EC concentrations over southern California are also higher than the observation. The overestimate over southern California is also shown in the RACM_SOA_VBS scheme. Similarly, the predicted sulfate concentrations over southern California are much higher than the observation too. Also, the surface sulfate concentrations throughout the U.S. are much higher than those of observations. In the FIM-Chem model, the anthrophonic emissions are from the HTAP v2.1 inventory, which based on the NEI2005 over United States. However, the BC emissions have declined by 50% in California from 1980 to 2008 following a parallel trend the reduction of fossil fuel BC emissions [Bahadur et al., 2011]. The older emission inventory with relatively higher anthropogenic emissions of BC and SO_2 may possibly induce the overestimates of near- surface BC and sulfate concentrations for the 2016 simulation in the model results over southern California and other areas. For the sulfate concentrations at upper levels, the GOCART (see

1   Fig. 10b the second column) scheme using the background fields of H_2O_2, OH and NO_3 shows much better
2   performance in capturing the relatively lower sulfate at upper levels than the other two gas-phase schemes.
3   This finding needs further analysis. For the gas species we compare CO, HCHO and O_3 (see Fig. 11) using
4   the RACM_GOCART and RACM_SOA_VBS schemes with the observation. Generally, the model cases
5   using either RACM_GOCART or RACM_SOA_VBS scheme show good performance in capturing the CO
6   and HCHO mixing ratios both at the surface and in the free troposphere. But they are both higher than the
7   observations near the surface over southern California, similar to EC and sulfate concentrations. This may
8   be also associated with the overestimation of anthropogenic emissions in the NEI-2005 over United States
9   for the year of 2016. Since CO and HCHO are precursors for O_3 production, the simulated O_3 also shows
10   slight enhancements compared to the observations that may be due to the higher CO and HCHO. Other than
11   that, the model is able to reproduce the O_3 profile over the US reasonably well, including the O_3 stratospheric
12   intrusions at the upper levels.

13   Figure 12 focuses on the 4th vertical profile over Kansas on August 23rd, 2016. The model results with
14   different chemical schemes are very consistent in simulating the meteorological fields. The modeled
15   temperature and virtual potential temperature show nearly exact agreement with the observations. But there
16   are still some shortcomings in forecast water vapor and relative humidity, especially above 6 km, where the
17   model results are overpredicted by nearly a factor of 2 and with less vertical variability. The vertical trend of
18   modeled wind speed and wind direction are close to the observed changes that increase with altitude. Similar
19   to Figure 9, the EC vertical profile using the RACM_SOA_VBS scheme, without the hydrophobic
20   assumption in wet removal, is similar to that of the observations while the other 2 schemes significantly
21   overpredict. Both the observations and models show decreasing vertical trend for sea salt and dust. The
22   GOCART scheme is able to reproduce the sulfate, except for the underestimate at 1.5-3 km. Otherwise, it
23   almost overlaps the observed profile at the upper levels. The O_3 vertical profile is reproduced by the model
24   using both RACM_GOCART and RACM_SOA_VBS schemes except a slight peak near 9 km where the
25   model is not able to capture the enhanced variability. The CO measurements have more fluctuations, but the
26   model roughly shows the major features of the vertical changes with altitude.

27   **5 Correlations between FIM-Chem model and ATom-1 observations**

28   For the aerosol size range of the GOCART scheme, the PALMS dataset allows for model evaluation of the
29   default sea salt emission algorithms by summing those bins less than 3 μm in the model results. The
30   comparison between the GOCART forecasts and ATom-1 data for all sea salt observations below 6 km are
31   shown in Figure 13. Different colors show different flight dates from August 15th (blue dots), 17th (green
32   dots), 20th (orange), 22nd (red) and 23rd (purple). Generally, modeled sea salt appears too high, especially on
33   flights of August 15th (blue dots), 20th (orange dots) and 23rd (purple dots) above ~4km. Some high values
34   below ~4km are reproduced by the models on the flight of August 17th (green dots). Some of the disagreement
35   may be due to uncertainties in the size range of sea salt observations, particularly the upper cutoff of 3 um
36   that is approximate (Murphy et al., 2019).

1   We also investigate the relationships of some key species for the biomass burning plumes observed on

2   8/15/17 and 8/17/17 between 22°S to 22°N below 6km (Fig. 14) for the RACM_SOA_VBS scheme. The

3   color bar indicates the latitude from south to north. Relative to CO, the model biomass burning emission

4   ratios are reasonable for EC with the modeled ratio (black color dots) somewhat lower than the observations

5   (color dots). However, the ratio of NO_y to CO is apparently too high in the fire emission processor. O_3

6   formation in the model plume is highly underpredicted (Fig. 14c and d), which is probably related to VOC

7   emission uncertainties within the fire emission ratio specifications.

8   **6 Conclusions**

9   A two way fully inline coupled global weather -chemistry prediction model FIM-Chem has been developed

10   at NOAA/ESRL/GSL to forecast the chemical composition and quantify the impacts on NWP. Three different

11   gas/aerosol chemistry schemes - GOCART, RACM_GOCART and RACM_SOA_VBS from WRF-Chem

12   have been implemented into FIM-Chem with some modifications as different options of chemical schemes.

13   In this study, the evaluation and analysis of model performance are focused on the fire events over Atlantic

14   from south to north on August 15th and 17th 2016 and the flight over United States from Minnesota to southern

15   California according to the NASA ATom-1 observations. The major conclusions are summarized as follows:

16   Compared with the explicitly simulated instantaneous H_2O_2, OH and NO_3 in RACM_GOCART mechanism,

17   there are about 10 $\mu g/m^3$ enhancements of sulfate and 15 $\mu g/m^3$ enhancements of $PM_{2.5}$ over the eastern US

18   and more than 20 μg enhancements of $PM_{2.5}$ over eastern China in the GOCART scheme, which has a simple

19   parameterization of sulfur/sulfate chemistry using prescribed background fields of OH, H_2O_2 and NO_3 to

20   calculate the sulfate production. Simulated instantaneous H_2O_2 is lower by 20% over eastern US and 40-60%

21   over India and eastern Asia, while the OH is 80% lower over eastern China in the RACM_GOCART scheme.

22   The GOCART and RACM_GOCART results are very consistent in forecasting sulfate, sea salt and EC due

23   to the same aerosol mechanism. For the fire events sampled over the Atlantic, the model shows very good

24   performance in reproducing the profiles of EC, CO, and O_3, especially in capturing the biomass burning

25   plumes near the equatorial areas (Fig. 6). However, for EC the RACM_SOA_VBS scheme shows much

26   better performance than that of the GOCART and RACM_GOCART schemes at the upper levels. That is

27   because it assumed that there is no wet deposition for hydrophobic BC in the GOCART and

28   RACM_GOCART schemes, which results into an underestimate of EC wet removal and overestimate of EC

29   concentrations at higher levels. The CO mixing ratio above ~2 km is underestimated over the tropics, which

30   may be related to lower simulated fire injection heights in the model. Otherwise, the general CO profiles are

31   well reproduced. The model using both RACM_GOCART and RACM_SOA_VBS schemes are able to

32   consistently reproduce O_3 mixing ratios, including the stratospheric intrusions above ~9 km at 40°S. There

33   is some slight underestimation of O_3 near the tropics, which might be associated with the underprediction of

34   CO. Meanwhile, we also evaluated other gas-phase species of CH_2O, OH and H_2O_2, which are important

35   precursors to many other chemical species within the RACM_GOCART and RACM_SOA_VBS schemes

1   (see Fig. 7). Generally, the pattern of the modeled HCHO, OH and H2O2 mixing ratio are almost the same

2   as that of the ATom-1 observations except for some underestimates above 9 km for HCHO and OH at some

3   latitudes, and some overestimates of H_2O_2 above 6 km in the southern hemisphere.

4   All of the chemical schemes are able to reproduce the general vertical gradients seen in the observations. The

5   RACM_SOA_VBS scheme is able to reproduce the vertical profile of EC much better than that of the

6   GOCART and RACM_GOCART schemes, which overestimate the EC concentrations above 2-4 km due to

7   the assumption of no wet deposition for hydrophobic BC. This comparison highlights the value of the ATom

8   data in examining basic assumptions within the wet removal parametrization of carbonaceous aerosol in the

9   GOCART mechanism. Results from the RACM_GOCART and RACM_SOA_VBS schemes show

10   consistency with observed O_3 and CO vertical profiles during the fire events. Both schemes show a slight

11   enhancement of O_3 at 1.5 km even though it underestimates the magnitude of the observed peak. For CO, the

12   model results capture the peak at about 2 km very well but overestimates the mixing ratio by about 30% near

13   the surface.

14   For the gas-phase species, the model either using the RACM_GOCART or RACM_SOA_VBS scheme

15   shows very good ability in forecasting the CO, O_3 and HCHO mixing ratio both at the surface and free

16   troposphere, including the O_3 stratospheric intrusions at the upper levels (Fig. 11). For EC and CO, a

17   precursor for O_3 production, there appears to be overestimated emissions over California causing much higher

18   surface mixing ratios in the forecasts than observed. For the comparisons of vertical profiles over California

19   on August 23rd 2016, the modeled meteorological fields of temperature and potential temperature show

20   agreement with the observations. The modeled water vapor and relative humidity are consistent with

21   observations below 6 km though they are overestimated above 6km. The RACM_SOA_VBS scheme shows

22   the best agreement with EC. For sulfate, the GOCART scheme is almost the same as the observation above

23   3km while it overestimates near the surface due to the high anthropogenic emissions used within the

24   inventory. The simulated O_3 and CO vertical profiles almost overlap the ATom-1 measurements but with

25   less vertical variability. Though data is somewhat sparse in our analysis, the sea salt emission algorithm

26   appears to be a model component that could be improved due to apparent consistent overestimation.

27   The comparison in this study successfully demonstrates that the FIM-Chem model with three difference

28   chemical schemes show good performance in forecasting the chemical composition for both aerosol and gas-

29   phase tracers when compared with the high temporal resolution (1-second) observations of ATom-1. The wet

30   removal assumption for hydrophobic BC is not reasonable, which need to be improved in the GOCART and

31   RACM_GOCART schemes. Thus, it is not necessary to use the complexity of a gas-phase scheme if the

32   focus is only on aerosol forecasts, in order to save time and computer resources. Using anthropogenic

33   emissions for the specific year of the simulation may help to improve the forecasts. Also, a new dynamic

34   core of Finite-volume cubed-sphere dynamical core (FV3) developed by GFDL will be used to replace of

35   FIM and coupled with the chemical schemes in the next generation global prediction system (NGGPS), as

36   FV3GFS-Chem, by using that to demonstrates the chemical impacts on NWP.

1   **Code and data availability**

2   Basically, the chemical modules of GOCART, RACM_GOCART and RACM_SOA_VBS are based on the
3   WRF-Chem   3.7,   which   can   be   obtained   from
4   http://www2.mmm.ucar.edu/wrf/users/download/get_source.html. The FIM-Chem_v1 code and model
5   configuration for chemical composition forecast here are available at https://github.com/NOAA-GSL/FIM-
6   Chem_v1. ATom-1 data is publicly available at the Oak Ridge National Laboratory Distributed Active
7   Archive Center: https://daac.ornl.gov/ATOM/guides/ATom_merge.html (Wofsy et al., 2018).

8   **Author contribution**

9   Li Zhang and Georg A. Grell developed the model coupling code and implemented the chemical modules
10   from WRF-Chem into FIM model. Li Zhang designed the experiments and performed the simulations. Stuart
11   A. McKeen evaluated the model performance and provided the suggestions to improve model performance.
12   Ravan Ahmadov developed the RACM-SOA-VBS scheme in WRF-Chem. Karl D. Froyd and Daniel
13   Murphy performed the measurements and provided the measured data of ATom-1 experiments. Li Zhang
14   prepared the manuscript with contributions from all co-authors.

15   **Competing interests**

16   The authors declare that they have no conflict of interest.

17   **Acknowledgements**

18   NOAA's next generation global prediction system (NGGPS) grant. Li Zhang, Stuart A. McKeen, Ravan
19   Ahmadov, and Karl Froyd are supported by funding from NOAA Award Number NA17OAR4320101.

1 **Reference**

2 Ahmadov, R., McKeen, S. A., Robinson, A., Bahreini, R., Middlebrook, A., Gouw, de J., Meagher, J., Hsie,
3 E., Edgerton, E., Shaw, S., Trainer, M.: A volatility basis set model for summertime secondary organic
4 aerosols over the eastern United States in 2006, J. Geophys. Res., 117, D06301, doi:10.1029/2011JD016831,
5 2012

6 Ahmadov R, Grell G, James E, Csiszar I, Tsidulko M, Pierce B, et al. Using VIIRS Fire Radiative Power
7 data to simulate biomass burning emissions, plume rise and smoke transport in a real-time air quality
8 modeling system. 2017 Ieee International Geoscience and Remote Sensing Symposium. IEEE International
9 Symposium on Geoscience and Remote Sensing IGARSS. New York: Ieee; 2017. p. 2806-8.

10 Andreae, M. O., Artaxo, P., Fischer, H., Freitas, S. R., Ǵregoire, J.-M., Hansel, A., Hoor, P., Kormann, R.,
11 Krejci, R., Lange, L., Lelieveld, J., Lindinger, W., Longo, K., Peters, W., de Reus, M., Scheeren, B., Silva
12 Dias, M. A. F., Strom, J., van Velthoven, P. F. J, and Williams, J.: Transport of biomass burning smoke to
13 the upper troposphere by deep convection in the equatorial region, Geophys. Res. Lett., 28(6), 951–954, 2001.

14 Balkanski, Y. J., Jacob, D. J., Gardner, G. M., Graustein, W. C., and Turekian, K. K.: Transport and residence
15 times of tropospheric aerosols inferred from a global three-dimensional simulation of ^{210}Pb, J. Geophys. Res.,
16 98, 20573, https://doi.org/10.1029/93JD02456, 1993.

17 Barnard, J. C., Fast, J. D., Paredes-Miranda, G., Arnott, W. P. and Laskin, A.: Technical note: evaluation of
18 the WRF-Chem 'aerosol chemical to aerosol optical properties' module using data from the MILAGRO
19 campaign. Atmos. Chem. Phys. 10, 7325–7340, 2010

20 Bauer, S. E., *and* Menon, S.: Aerosol direct, indirect, semidirect, and surface albedo effects from sector
21 contributions based on the IPCC AR5 emissions for preindustrial and present-day conditions, *J. Geophys.*
22 *Res.,* 117, *D01206, doi:*10.1029/2011JD016816, 2012

23 Bleck, R., Bao, J., Benjamin, G. S., Brown, M. J., Fiorino, M., Henderson, B. T., Lee, J., MacDonald, E. A.,
24 Madden, P., Middlecoff, J., Rosinski, J., Smirnova, T., G. Sun, S., and Wang, N.: A Vertically Flow-
25 Following Icosahedral Grid Model for Medium-Range and Seasonal Prediction. Part I: Model Description.
26 Mon. Wea. Rev., 143, 2386–2403, doi: 10.1175/MWR-D-14-00300.1, 2015

27 Bourgeois, I., Peischl, J., Thompson, C. R., Aikin, K. C., Campos, T., Clark, H., Commane, R., Daube, B.,
28 Diskin, G. W., Elkins, J. W., Gao, R.-S., Gaudel, A., Hintsa, E. J., Johnson, B. J., Kivi, R., McKain, K.,
29 Moore, F. L., Parrish, D. D., Querel, R., Ray, E., Sánchez, R., Sweeney, C., Tarasick, D. W., Thompson, A.
30 M., Thouret, V., Witte, J. C., Wofsy, S. C., and Ryerson, T. B.: Global-scale distribution of ozone in the
31 remote troposphere from the ATom and HIPPO airborne field missions, Atmos. Chem. Phys., 20, 10611–
32 10635, https://doi.org/10.5194/acp-20-10611-2020, 2020.

33 Brioude, J., et al.: Top-down estimate of anthropogenic emission inventories and their interannual variability
34 in Houston using a mesoscale inverse modeling technique, J. Geophys. Res., 116, *D20305,*
35 *doi:*10.1029/2011JD016215, 2011

36 Brown-Steiner, B., Hess, P. G., and Lin, M. Y.: On the capabilities and limitations of GCCM simulations of
37 summertime regional air quality: A diagnostic analysis of ozone and temperature simulations in the US using
38 CESM CAM-Chem, Atmos. Environ., 101, 134–148, doi:10.1016/j.atmosenv.2014.11.001, 2015.

39 Canty, T. P., Hembeck, L., Vinciguerra, T. P., Anderson, D. C., Goldberg, D. L., Carpenter, S. F., Allen, D.
40 J., Loughner, C. P., Salawitch, R. J., and Dickerson, R. R.: Ozone and NOx chemistry in the eastern US:
41 evaluation of CMAQ/CB05 with satellite (OMI) data, Atmos. Chem. Phys., 15, 10965–10982,
42 doi:10.5194/acp-15-10965-2015, 2015.

43 Carlton, A. G., Bhave, V. P., Napelenok, L. S., Edney, D. E., Sarwar, G., Pinder, W. R., Pouliot, A. G., and
44 Houyoux, M.: Model Representation of Secondary Organic Aerosol in CMAQv4.7, *Environmental Science*
45 *& Technology*, *44*(22), 8553-8560, 2010.

46 Chen, F., and Dudhia, J.: Coupling an advanced land surface-hydrology model with the Penn State-NCAR
47 MM5 modeling system. Part I: Model implementation and sensitivity. Mon. Wea. Rev., 129, 569-585, 2001.

1 Chen, Q., Yin, Y., Jin, L.-J., Xiao, H., Zhu, S.-Ch.: The effect of aerosol layers on convective cloud
2 microphysics and precipitation, Atmos. Res., 101 (1-2), pp. 327–
3 340 http://doi.org/10.1016/j.atmosres.2011.03.007, 2011.

4 Chin, M., Rood, B. R., Lin, S.-J., Muller, F. J., and Thomspon, M. A.: Atmosphericsulfur cycle in the global
5 model GOCART: Model description and global properties, J. Geophys. Res., 105, 24,671-24,687, 2000.

6 Colarco, P. R., Nowottnick, E. P., Randles, C. A., Yi, B., Yang, P., Kim, K. M., Smith, J. A. and Bardeen, C.
7 G.: Impact of radiatively interactive dust aerosols in the NASA GEOS-5 climate model: Sensitivity to dust
8 particle shape and refractive index. J. Geophys. Res. Atmos. 119: 753–786, 2014.

9 Ek, M. B., Mitchell, K. E., Lin, Y., Rogers, E., Grunmann, P., Koren, V., Gayno, G., and Tarpley, J. D., 2003:
10 Implementation of Noah land surfacemodel advances in the National Centers for Environmental Prediction
11 operational mesoscale Eta model. J. Geophys. Res., 108, 8851–8866, doi:10.1029/2002JD003296, 2003.

12 Erisman, J.W, and Pul, V. A.: Parameterization of surface resistance for the quantification of atmospheric
13 deposition of acidifying pollutants and ozone, Atmos. Environ, 28, 2595-2607, 1994.

14 Fast, J. D., Gustafson Jr., I. W., Easter, C. R., Zaveri, A. R., Barnard, C. J., Chapman, G. E., Grell, A. G.,
15 and Peckham, E. S.: Evolution of ozone, particulates, and aerosol direct radiative forcing in the vicinity of
16 Houston using a fully coupled meteorology-chemistry-aerosol model. J. Geophys. Res., 111, D21305,
17 doi:10.1029/2005JD006721, 2006.

18 Fiore, A. M., et al.: Multimodel estimates of intercontinental source-receptor relationships for ozone pollution,
19 *J. Geophys. Res.*, 114, D04301, doi:10.1029/2008JD010816, 2009.

20 Fiore, A. M., Horowitz, L. W., Purves, D. W., Levy, H., Evans, M. J., Wang, Y., Li, Q., and Yantosca, R.:
21 Evaluating the contribution of changes in isoprene emissions to surface ozone trends over the eastern United
22 States, J. Geophys. Res., 110, D12303, doi:10.1029/2004jd005485, 2005.

23 Freitas, S. R., Longo, K. M., Alonso, M. F., Pirre, M., Marecal, V., Grell, G., Stockler, R., Mello, R. F., and
24 Sánchez Gácita, M.: PREP-CHEM-SRC – 1.0: a preprocessor of trace gas and aerosol emission fields for
25 regional and global atmospheric chemistry models, Geosci. Model Dev., 4, 419-433, doi:10.5194/gmd-4-
26 419-2011,   2011.
27 Froyd, K. D., Murphy, D. M., Brock, C. A., Campuzano-Jost, P., Dibb, J. E., Jimenez, J.-L., Kupc, A.,
28 Middlebrook, A. M., Schill, G. P., Thornhill, K. L., Williamson, C. J., Wilson, J. C., and Ziemba, L. D.: A
29 new method to quantify mineral dust and other aerosol species from aircraft platforms using single-particle
30 mass spectrometry, Atmos. Meas. Tech., 12, 6209–6239, https://doi.org/10.5194/amt-12-6209-2019, 2019.

31 Giglio, L., Descloitres, J., Justice, C. O., and Kaufman, Y. J.: An enhanced contextual fire detection algorithm
32 for MODIS, RemoteSens. Environ., 87, 273–282, 2003.

33 Giorgi, F., and Chameides, L. W.: Rainout lifetimes of highly soluble aerosols and gases as inferred from
34 simulations with a general circulation model. *J. Geophys. Res.*, **91**, 14367–14376, 1986.

35 Grell, G. A., and Dévényi, D.: A generalized approach to parameterizing convection combining ensemble
36 and data assimilation techniques, *Geophys. Res. Lett.*, 29(14), doi:10.1029/2002GL015311, 2002.

37 Grell, G. A., Peckham, E. S., Schmitz, R., McKeen, A. S., Frost, G., Skamarock, W., and Eder, B.: Fully-
38 coupled online chemistry within the WRF model. *Atmospheric Environment*, **39**, 6957-6975,
39 doi:10.1016/j.atmosenv.2005.04.027, 2005.

40 Grell, G., Freitas, S. R., Stuefer, M., and Fast, J.: Inclusion of biomass burning in WRF-Chem: impact of
41 wildfires on weather forecasts, Atmos. Chem. Phys., 11, 5289-5303, https://doi.org/10.5194/acp-11-5289-
42 2011, 2011.

43 Grell, G. A. and Freitas, S. R.: A scale and aerosol aware stochastic convective parameterization for weather
44 and air quality modeling, Atmos. Chem. Phys., 14, 5233–5250, https://doi.org/10.5194/acp-14-5233-2014,
45 2014.

46 Hallquist, M., Wenger, J. C., Baltensperger, U., Rudich, Y., Simpson, D., Claeys, M., Dommen, J., Donahue,
47 N. M., George, C., Goldstein, A. H., Hamilton, J. F., Herrmann, H., Hoffmann, T., Iinuma, Y., Jang, M.,
48 Jenkin, M. E., Jimenez, J. L., Kiendler-Scharr, A., Maenhaut, W., McFiggans, G., Mentel, Th. F., Monod,

A., Prévôt, A. S. H., Seinfeld, J. H., Surratt, J. D., Szmigielski, R., and Wildt, J.: The formation, properties and impact of secondary organic aerosol: current and emerging issues, Atmos. Chem. Phys., 9, 5155-5236, https://doi.org/10.5194/acp-9-5155-2009, 2009.

Haustein, K., Pérez, C., Baldasano, J. M., Jorba, O., Basart, S., Miller, R. L., Janjic, Z., Black, T., Nickovic, S., Todd, M. C., Washington, R., Müller, D., Tesche, M., Weinzierl, B., Esselborn, M., and Schladitz, A.: Atmospheric dust modeling from meso to global scales with the online NMMB/BSC-Dust model – Part 2: Experimental campaigns in Northern Africa, Atmos. Chem. Phys., 12, 2933-2958, https://doi.org/10.5194/acp-12-2933-2012, 2012.

Janjic, Z. I. Pressure gradient force and advection scheme used for forecasting with steep and small scale topography. Beitr. Phys. Atmos., 50, 186–199, 1977.

Janssens-Maenhout, G., Crippa, M., Guizzardi, D., Dentener, F., Muntean, M., Pouliot, G., Keating, T., Zhang, Q., Kurokawa, J., Wankmüller, R., Denier van der Gon, H., Kuenen, J. J. P., Klimont, Z., Frost, G., Darras, S., Koffi, B., and Li, M.: HTAP_v2.2: a mosaic of regional and global emission grid maps for 2008 and 2010 to study hemispheric transport of air pollution, Atmos. Chem. Phys., 15, 11411-11432, https://doi.org/10.5194/acp-15-11411-2015, 2015.

Koren, V., Schaake, J., Mitchell, K., Duan, Q.-Y., Chen, F., and Baker, J. M.: A parameterization of snowpack and frozen ground intended for NCEP weather and climate models. J. Geophys. Res., 104, 19 569–19 585, doi:10.1029/1999JD900232, 1999.

Kok, J. F.: A scaling theory for the size distribution of emitted dust aerosols suggests climate models underestimate the size of the global dust cycle, *Proceedings of the National Academy of Sciences (PNAS)*, 108(3), 1016-21, 2011

LeGrand, S. L., Polashenski, C., Letcher, T. W., Creighton, G. A., Peckham, S. E., and Cetola, J. D.: The AFWA dust emission scheme for the GOCART aerosol model in WRF-Chem v3.8.1, Geosci. Model Dev., 12, 131-166, https://doi.org/10.5194/gmd-12-131-2019, 2019.

Levin, Z., and Cotton R. W.: Aerosol Pollution Impact on Precipitation, Aerosol Pollution Impact on Precipitation: A Scientific Review, 407 pp., Springer, New York, 2009.

Lin, J., Youn, D., Liang, X., and Wuebbles, D.: Global model simulation of summertime U.S. ozone diurnal cycle and its sensitivity to PBL mixing, spatial resolution, and emissions, Atmos. Environ., 42, 8470–8483, doi:10.1016/j.atmosenv.2008.08.012, 2008.

Lin, Y.-L., Farley, D. R., and Orville, D. H.: Bulk parameterization of the snow field in a cloud model. *J. Climate Appl. Meteor.*, **22**, 1065–1092, doi:https://doi.org/10.1175/1520-0450(1983)022<1065:BPOTSF>2.0.CO;2, 1983.

Longo, K. M., Freitas, S. R., Andreae, M. O., Setzer, A., Prins, E., and Artaxo, P.: The Coupled Aerosol and Tracer Transport model to the Brazilian developments on the Regional Atmospheric Modeling System (CATT-BRAMS) – Part 2: Model sensitivity to the biomass burning inventories, Atmos. Chem. Phys., 10, 5785–5795, doi:10.5194/acp-10-5785-2010, 2010.

Marticorena, B. and Bergametti, G.: Modeling the atmospheric dust cycle: 1-Design of a soil derived dust production scheme, J. Geophys. Res., 100, 16415-16430, 1995.

McDonald-Buller, E. C., Allen, D. T., Brown, N., Jacob, D. J., Jaffe, D., Kolb, C. E., Lefohn, A. S., Oltmans, S., Parrish, D. D., Yarwood, G., and Zhang, L.: Establishing policy relevant background (PRB) ozone concentrations in the United States, Enviriron. Sci. Technol., 45, 9484–9497, doi:10.1021/es2022818, 2011.

Muhlbauer, A., Grabowski, W. W., Malinowski, P. S., Ackerman, P. T., Bryan, H. G., Lebo, J. Z., Milbrandt, A. J., Morrison, H., Ovchinnikov, M., Tessendorf, S., Thériault, G. J.M.: Thompson Reexamination of the state of the art of cloud modelling shows real improvements, Bull. Am. Meteorol. Soc., 94, pp. ES45–ES48 http://doi.org/10.1175/BAMS-D-12-00188.1, 2013.

Mulcahy, J. P., Walters, D. N., Bellouin, N., and Milton, S. F.: Impacts of increasing the aerosol complexity in the Met Office global numerical weather prediction model, Atmos. Chem. Phys., 14, 4749-4778, doi:10.5194/acp-14-4749-2014, 2014.

Murphy, D. M., Cziczo, J. D., Froyd, D. K., Hudson, K. P., Matthew, M. B., Middlebrook, M. A., Peltier, R., Sullivan, A. E., Thomson, S. D., and Weber J. R.: Single-particle mass spectrometry of tropospheric aerosol particles, *J. Geophys. Res.*, 111, D23S32, doi: 10.1029/2006JD007340, 2006.

Murphy, D. M., Froyd, K. D., Schwarz, J. P., Wilson, J.C.: The chemical composition of stratospheric aerosol particles. Q. J. R. Meteorol. Soc. 140, 1269–1278. http://dx. doi.org/10.1002/qj.2213., 2014.

Murphy, D., Froyd, K., Apel, E.,Blake, R. D., Blake, J. N., Evangeliou, N., Hornbrook, S. R., Peischl, J., Ray, E., Ryerson,B. T., Thompson, C., and Stohl, A.: An aerosol particle containing enriched uranium encountered in the remote T upper troposphere, *J. Environ. Radioactivity, 184–185*, 95-100, doi:10.1016/j.jenvrad.2018.01.006, 2018

Murphy, D. M., Froyd, K. D., Bian, H., Brock, C. A., Dibb, J. E., DiGangi, J. P., Diskin, G., Dollner, M., Kupc, A., Scheuer, E. M., Schill, G. P., Weinzierl, B., Williamson, C. J., and Yu, P.: The distribution of sea-salt aerosol in the global troposphere, Atmos. Chem. Phys., 19, 4093–4104, https://doi.org/10.5194/acp-19-4093-2019, 2019

Myhre, G., Samset, B. H., Schulz, M., Balkanski, Y., Bauer, S., Berntsen, T. K., Bian, H., Bellouin, N., Chin, M., Diehl, T., Easter, R. C., Feichter, J., Ghan, S. J., Hauglustaine, D., Iversen, T., Kinne, S., Kirkevåg, A., Lamarque, J.-F., Lin, G., Liu, X., Lund, M. T., Luo, G., Ma, X., van Noije, T., Penner, J. E., Rasch, P. J., Ruiz, A., Seland, Ø., Skeie, R. B., Stier, P., Takemura, T., Tsigaridis, K., Wang, P., Wang, Z., Xu, L., Yu, H., Yu, F., Yoon, J.-H., Zhang, K., Zhang, H., and Zhou, C.: Radiative forcing of the direct aerosol effect from AeroCom Phase II simulations, Atmos. Chem. Phys., 13, 1853-1877, https://doi.org/10.5194/acp-13-1853-2013, 2013.

Peuch, V. H. et al. (Eds.).: MACC-II final report: Monitoring Atmospheric Composition and Climate-Interim Implementation (the European Union's Framework Programme under grant agreement number 283576) . Retrieved from https://atmosphere.copernicus.eu, 2014

Powers JG, Klemp JB, Skamarock WC, Davis CA, Dudhia J, Gill DO, et al. THE WEATHER RESEARCH AND FORECASTING MODEL Overview, System Efforts, and Future Directions. Bull Amer Meteorol Soc. 2017;98(8):1717-37.

Reale, O., Lau, K. M., and Silva da, A.: Impact of interactive aerosol on the African easterly jet in the NASA GEOS-5 Global Forecasting System. Wea. Forecasting, 26, 504–519, 2011.

Reidmiller, D. R., Fiore, A. M., Jaffe, D. A., Bergmann, D., Cuvelier, C., Dentener, F. J., Duncan, B. N., Folberth, G., Gauss, M., Gong, S., Hess, P., Jonson, J. E., Keating, T., Lupu, A., Marmer, E., Park, R., Schultz, M. G., Shindell, D. T., Szopa, S., Vivanco, M. G., Wild, O., and Zuber, A.: The influence of foreign vs. North American emissions on surface ozone in the US, Atmos. Chem. Phys., 9, 5027-5042, https://doi.org/10.5194/acp-9-5027-2009, 2009.

Rodwell, M. J. and Jung, T.: Understanding the local and global impacts of model physics changes: an aerosol example, Q.J.R. Meteorol. Soc., 134, 1479–1497, doi:10.1002/qj.298, 2008.

Sakaeda, N., Wood, R., and Rasch, J. P.: Direct and semidirect aerosol effects of southern African biomass burning aerosol, J. Geophys. Res., 116, D12205, doi:10.1029/2010JD015540, 2011.

Schill, G.P., Froyd, K.D., Bian, H. et al. Widespread biomass burning smoke throughout the remote troposphere. Nat. Geosci. 13, 422–4. https://doi.org/10.1038/s41561-020-0586-1, 2020

Schwarz, J. P., Samset, B. H., Perring, A. E., Spackman, J. R., Gao, R. S., Stier, P., Schulz, M., Moore, F. L., Ray, E. A., and Fahey, D. W.: Global-scale seasonally resolved black carbon vertical profiles over the Pacific, Geophys. Res. Lett., 40, 5542– 5547, doi:10.1002/2013GL057775, 2013

Stockwell, W. R., Kirchner, F., Kuhn, M., and Seefeld, S.: A new mechanism for regional atmospheric chemistry modeling, *J. Geophys. Res.-Atmos.*, *102*(D22), 25847-25879, 1997.

Stockwell, W. R., Kley, D.: The Euro-RADM Mechanism: A Gas-Phase Chemical Mechanism for European Air Quality Studies, Forschungszentrum Julich, Jtilich, Germany 1994.

Stockwell, W. R., Middleton, P., Chang, S. J., Tang X.: The second generation regional Acid Deposition Model chemical mechanism for regional air quality modeling, J. Geophys. Res., 95, 16,343-16,367, 1990.

Su, W.Y., Loeb, G. N., Schuster, L. G., Chin, M., Rose, G. F. : Global all-sky shortwave direct radiative forcing of anthropogenic aerosols from combined satellite observations and GOCART simulations, *J. Geophys. Res. - A*, 118, 2, 655-669, doi:10.1029/2012JD018294, 2013.

Sun, S., R. Bleck, S. G. Benjamin, B. W. Green, and G. A. Grell, 2018a: Subseasonal Forecasting with an Icosahedral, Vertically Quasi-Lagrangian Coupled Model. Part I: Model Overview and Evaluation of Systematic Errors. Mon. Wea. Rev., 146, 1601–1617, https://doi.org/10.1175/MWR-D-18-0006.1.

Sun, S., B.W. Green, R. Bleck, S.G. Benjamin, and G.A. Grell, 2018b: Subseasonal forecasting with an icosahedral, vertically quasi-Lagrangian coupled model. Part II: Probabilistic and deterministic forecast skill. Mon. Weather Rev., 146, no. 5, 1619-1639, doi:10.1175/MWR-D-18-0007.1

Thomson, D.S., Schein, M. E., Murphy, D.M.: Particle analysis by laser mass spectrometry WB-57F instrument overview. Aero. Sci. Technol. 33, 153–169, 2000.

Travis, K. R., Jacob, D. J., Fisher, J. A., Kim, P. S., Marais, E. A., Zhu, L., Yu, K., Miller, C. C., Yantosca, R. M., Sulprizio, M. P., Thompson, A. M., Wennberg, P. O., Crounse, J. D., St. Clair, J. M., Cohen, R. C., Laughner, J. L., Dibb, J. E., Hall, S. R., Ullmann, K., Wolfe, G. M., Pollack, I. B., Peischl, J., Neuman, J. A., and Zhou, X.: Why do models overestimate surface ozone in the Southeast United States?, Atmos. Chem. Phys., 16, 13561-13577, https://doi.org/10.5194/acp-16-13561-2016, 2016.

Wang, H., Rasch, J. P., Easter, C. R., Singh, B., Zhang, R., Ma, P.-L., Qian, Y., Ghan, J. S., and Beagley, N.: Using an explicit emission tagging method in global modeling of source receptor relationships for black carbon in the Arctic: Variations, sources, and transport pathways, J. Geophys. Res. Atmos., 119, 12,888–12,909, doi:10.1002/2014JD022297, 2014a

Wang, Q., Jacob, J. D., Spackman, R. J., Perring, E. A., Schwarz, P. J., Moteki, N., Marais, A. E., Ge, C., Wang, J., and Barrett, R. H. S.: Global budget and radiative forcing of black carbon aerosol: Constraints from pole-to-pole (HIPPO) observations across the Pacific, J. Geophys. Res. Atmos., 119, 195–206, doi:10.1002/2013JD020824, 2014b

Wesely, M. L.: Parameterization of surface resistance to gaseous dry deposition in regional-scale numerical models, Atmos. Environ., 23, 1293–1304, 1989.

Westphal, D. L.*, and* Toon, B. O.: Simulations of microphysical, radiative, and dynamical processes in a continental-scale forest fire smoke plume*, J. Geophys. Res., 96(*D12*), 22379–22400, doi:10.1029/91JD01956, 1991.

Wofsy, S. C., Afshar, S., Allen, H. M., Apel, E., Asher, E. C., Barletta, B., Bent, J., Bian, H., Biggs, B. C., Blake, D. R., Blake, N., Bourgeois, I., Brock, C. A., Brune, W. H., Budney, J. W., Bui, T. P., Butler, A., Campuzano-Jost, P., Chang, C. S., Chin, M., Commane, R., Correa, G., Crounse, J. D., Cullis, P. D., Daube, B. C., Day, D. A., Dean-Day, J. M., Dibb, J. E., Di- Gangi, J. P., Diskin, G. S., Dollner, M., Elkins, J. W., Erdesz, F., Fiore, A. M., Flynn, C. M., Froyd, K., Gesler, D. W., Hall, S. R., Hanisco, T. F., Hannun, R. A., Hills, A. J., Hintsa, E. J., Hoffman, A., Hornbrook, R. S., Huey, L. G., Hughes, S., Jimenez, J. L., Johnson, B. J., Katich, J. M., Keeling, R. F., Kim, M. J., Kupc, A., Lait, L. R., Lamarque, J.-F., Liu, J., McKain, K., Mclaughlin, R. J., Meinardi, S., Miller, D. O., Montzka, S. A., Moore, F. L., Morgan, E. J., Murphy, D. M., Murray, L. T., Nault, B. A., Neuman, J. A., Newman, P. A., Nicely, J. M., Pan, X., Paplawsky, W., Peischl, J., Prather, M. J., Price, D. J., Ray, E., Reeves, J. M., Richardson, M., Rollins, A. W., Rosenlof, K. H., Ryerson, T. B., Scheuer, E., Schill, G. P., Schroder, J. C., Schwarz, J. P., St.Clair, J. M., Steenrod, S. D., Stephens, B. B., Strode, S. A., Sweeney, C., Tanner, D., Teng, A. P., Thames, A. B., Thompson, C. R., Ullmann, K., Veres, P. R., Vieznor, N., Wagner, N. L., Watt, A., Weber, R., Weinzierl, B., Wennberg, P., Williamson, C. J., Wilson, J. C., Wolfe, G. M., Woods, C. T., and Zeng, L. H.: ATom: Merged Atmospheric Chemistry, Trace Gases, and Aerosols, ORNL DAAC, Oak Ridge, Ten- nessee, https://doi.org/10.3334/ornldaac/1581, 2018.

Xie, S. P., B. Lu, and Xiang, Q. B.: Similar spatial patterns of climate responses to aerosol and greenhouse gas changes. *Nat. Geosci.*, **6**, 828–832, doi:https://doi.org/10.1038/ngeo1931, 2013.

Yang, Q., Bitz, C. M., and Doherty, S. J.: Offsetting effects of aerosols on Arctic and global climate in the late 20th century, Atmos. Chem. Phys., 14, 3969-3975, https://doi.org/10.5194/acp-14-3969-2014, 2014.

1 Yu, P., Froyd, K. D., Portmann, R. W., Toon, O. B., Freitas, S. R., Bardeen, C. G., et al.: Efficient in-cloud
2 removal   of   aerosols   by   deep   convection. Geophysical   Research
3 Letters, 46, 1061– 1069. https://doi.org/10.1029/2018GL080544, 2019.

4 Zhang, Q., et al.: Ubiquity and dominance of oxygenated species in organic aerosols in anthropogenically-
5 influenced   Northern   Hemisphere   mid-latitudes,   Geophys.   Res.   Lett.,   34,   L13801,
6 doi:10.1029/2007GL029979, 2007.

7 Zhao, C., Liu, X., Leung, L. R., Johnson, B., McFarlane, S. A., Gustafson Jr., W. I., Fast, J. D., and Easter,
8 R.: The spatial distribution of mineral dust and its shortwave radiative forcing over North Africa: modeling
9 sensitivities to dust emissions and aerosol size treatments, Atmos. Chem. Phys., 10, 8821-8838,
10 https://doi.org/10.5194/acp-10-8821-2010, 2010.

1 **Figure captions.**

2 **Figure 1.** Vertical profiles and transect time series of the ATom-1 flight tracks on August 15th and 17th, 2016

3 over Atlantic Ocean and August 23rd 2006 over US.

4 **Figure 2.** 120 hours forecast of $PM_{2.5}$ and sulfate using (a) GOCART and (b) RACM_GOCART schemes,

5 and their (c) differences (RACM_GOCART minus GOCART) at 00Z July 29th 2016. Unit: μg /m^3.

6 **Figure 3.** Comparisons of H_2O_2, OH, and NO_3 between (a) GOCART and (b) RACM_GOCART schemes,

7 and their (c) differences (RACM_GOCART minus GOCART) at 00Z July 29th 2016. Unit: ppb

8 **Figure 4.** 120 hours forecast of surface O_3 using RACM_GOCART scheme at 12z August 2nd and 00z

9 August 3rd 2016. Unit: ppb

10 **Figure 5.** 120 hours forecast of surface SOA using RACM_SOA_VBS scheme at 12z August 2nd and 00z

11 August 3rd 2016. Unit: ug/m^3.

12 **Figure 6.** Height-latitude profiles of EC, CO and O_3 over Atlantic on August 15th and August 17th, 2016 for

13 (a) ATom-1; (b) RACM_GOCART; and (c) RACM_SOA_VBS.

14 **Figure 7.** Height-latitude profiles of HCHO, OH and H_2O_2 over Atlantic on August 15th and August 17th,

15 2016 for (a) ATom-1 observations; (b) RACM_GOCART; and (c) RACM_SOA_VBS.

16 **Figure 8.** ATom-1 observations and model results for temperature, virtual potential temperature, water vapor,

17 relative humidity, wind speed and wind direction in the (a) biomass burning and (b) dust events. The biomass

18 burning plume is from August 15, 2016, profile #16 near 20°S while the Saharan dust plume is from August

19 17, 2016, profile #10 near 25°N.

20 **Figure 9.** Comparisons between ATom-1 observations and model vertical profiles of EC, sea salt, dust, O_3

21 and CO in the biomass burning (a) and dust (b) events. The biomass burning plume is from August 15, 2016,

22 profile #16 near 20°S while the Saharan dust plume is from August 17, 2016, profile #10 near 25°N. Green

23 and blue lines are nearly identical for aerosol.

24 **Figure 10.** Height-latitude profiles of EC and sulfate over United States on August 23rd, 2016 for (a) ATom-

25 1; (b) GOCART; (c) RACM_GOCART; and (d) RACM_SOA_VBS.

26 **Figure 11.** Height-latitude profiles of CO, O_3 and HCHO over United States on August 23rd, 2016 for (a)

27 ATom-1; (b) RACM_GOCART; and (c) RACM_SOA_VBS.

28 **Figure 12.** Observations and model results for profile #4, 8/23/16 over southeastern Kansas.

29 **Figure 13.** GOCART model forecast versus ATom-1 observed sea salt below 6 km.

30 **Figure 14.** Model (black color dot) and observation (color dot) ratios of (a) EC relative to CO; (b) NO_y

31 relative to CO; (c) O_3 relative to CO and (d) O_3 relative to NO_y. Color scale is degree latitude.
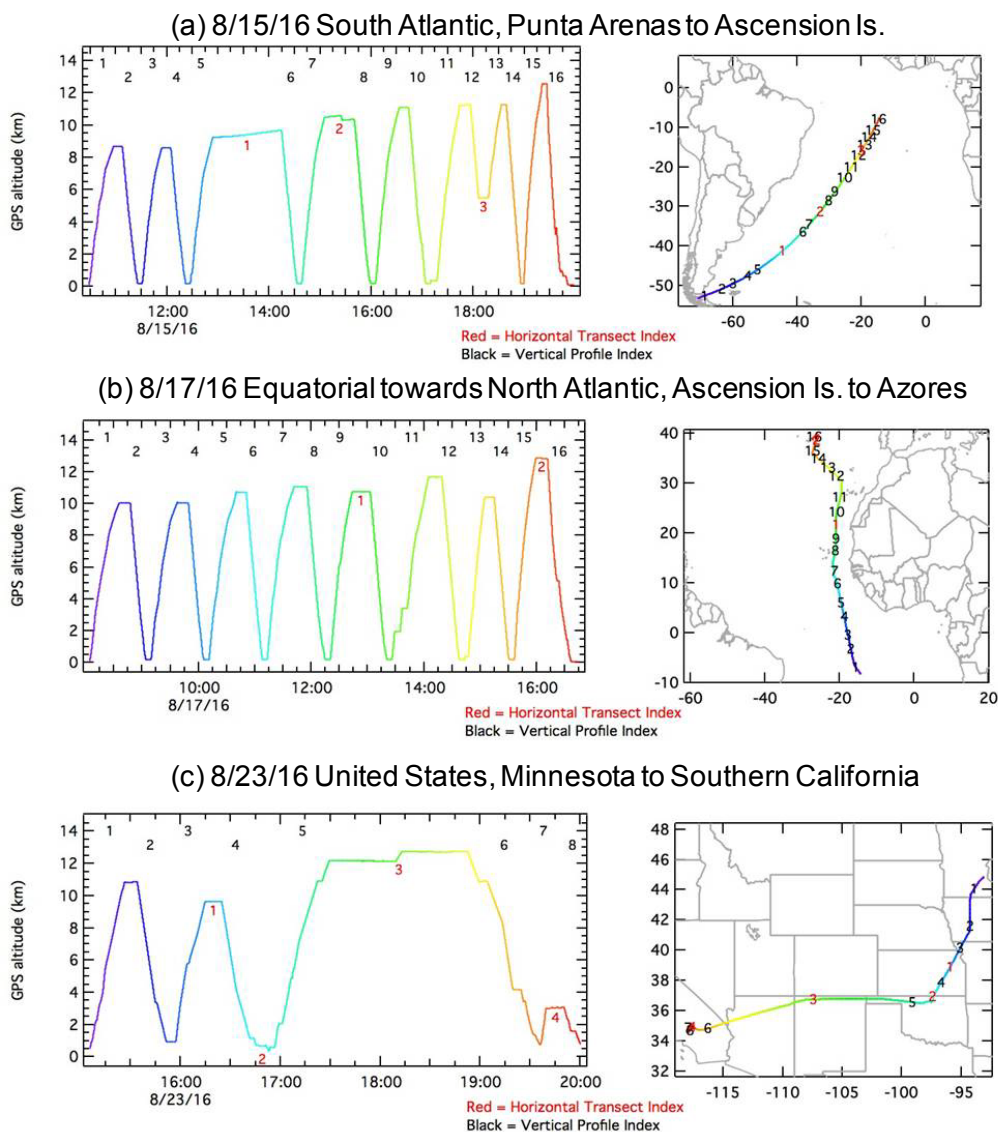
Figure 1: Vertical profiles and transect time series of the ATom-1 flight tracks on August 15th and 17th, 2016 over Atlantic Ocean and August 23rd 2006 over US.
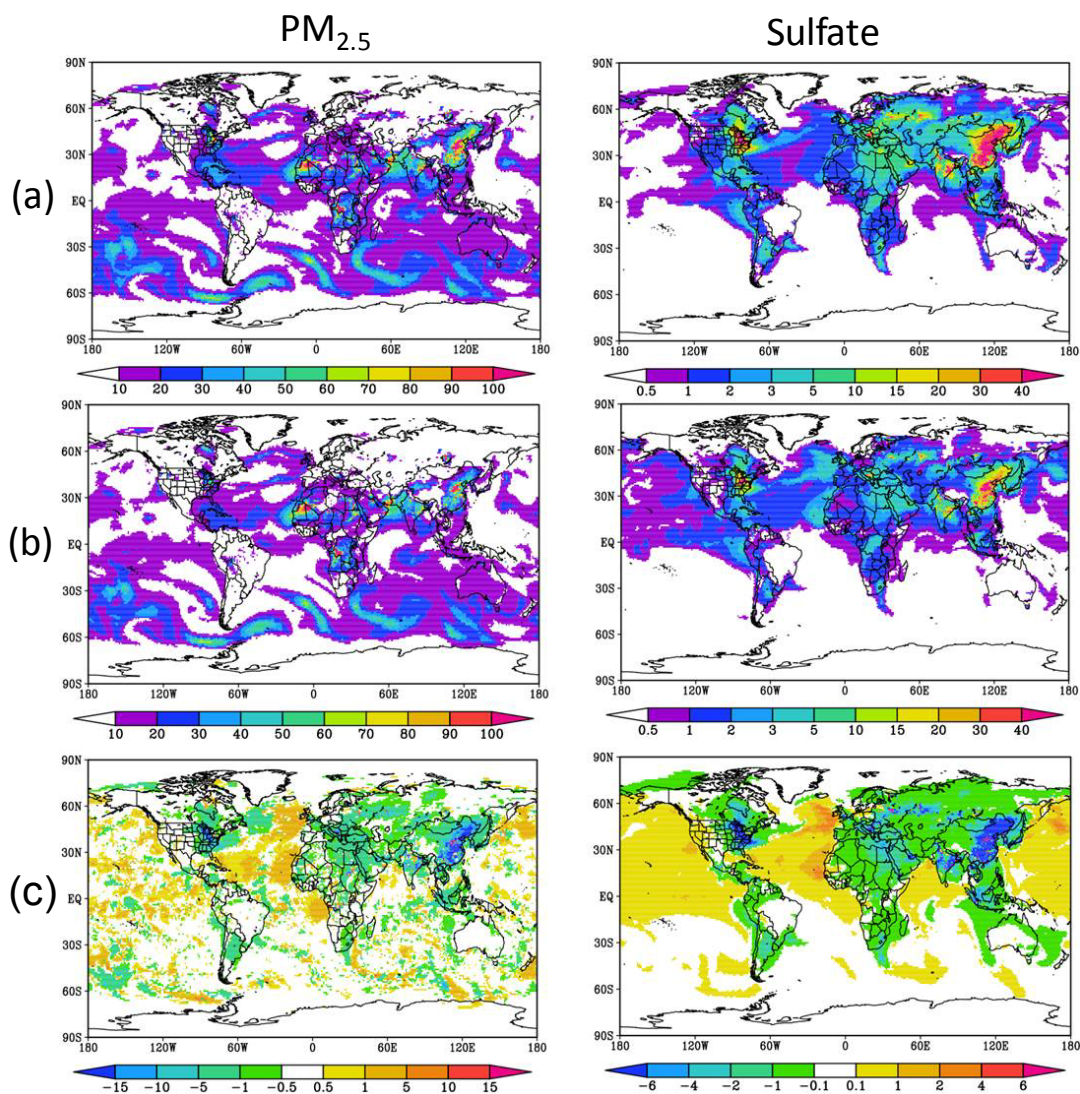
Figure 2: 120 hours forecast of PM2.5 and sulfate using (a) GOCART and (b) RACM_GOCART schemes, and their (c) differences (RACM_GOCART minus GOCART) at 00Z July 29th 2016. Unit: ?g /m3
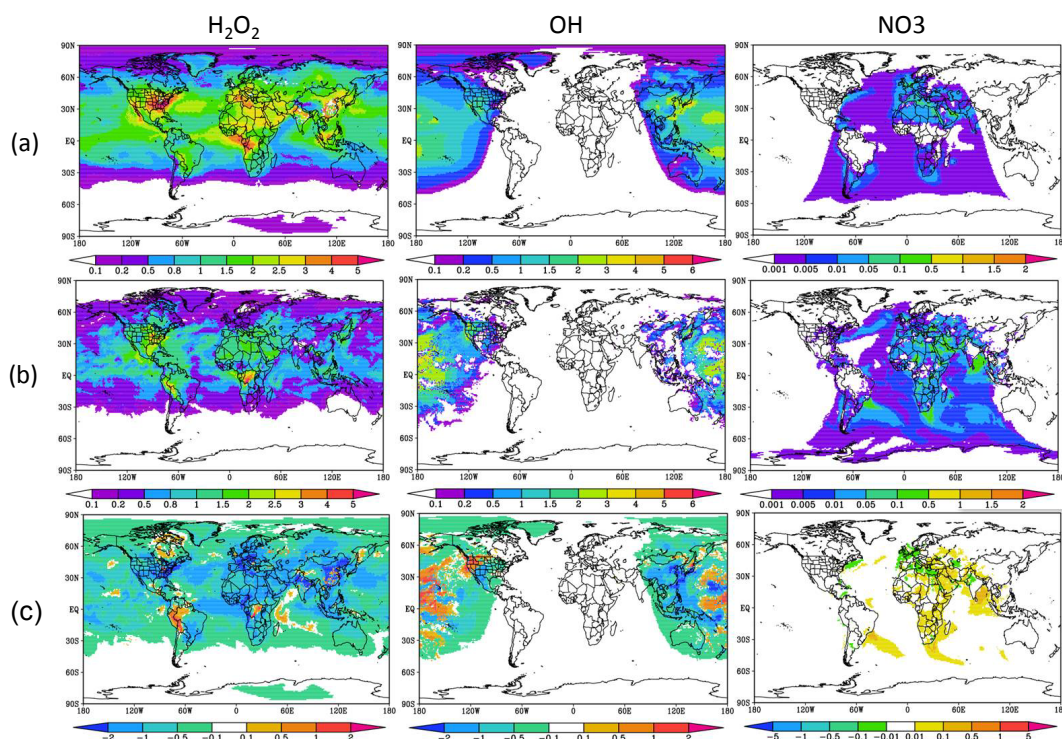
Figure 3: Comparisons of H2O2, OH, and NO3 between (a) GOCART and (b) RACM_GOCART schemes, and their (c) differences (RACM_GOCART minus GOCART) at 00Z July 29th 2016.
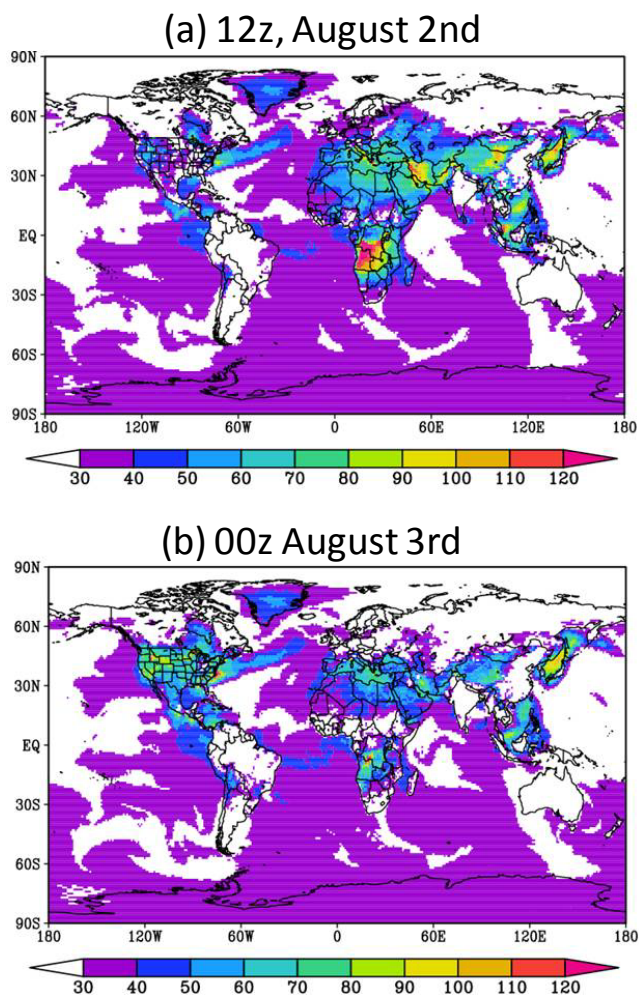
Figure 4: 120 hours forecast of surface O3 using RACM_GOCART scheme at 12z August 2nd and 00z August 3rd 2016.
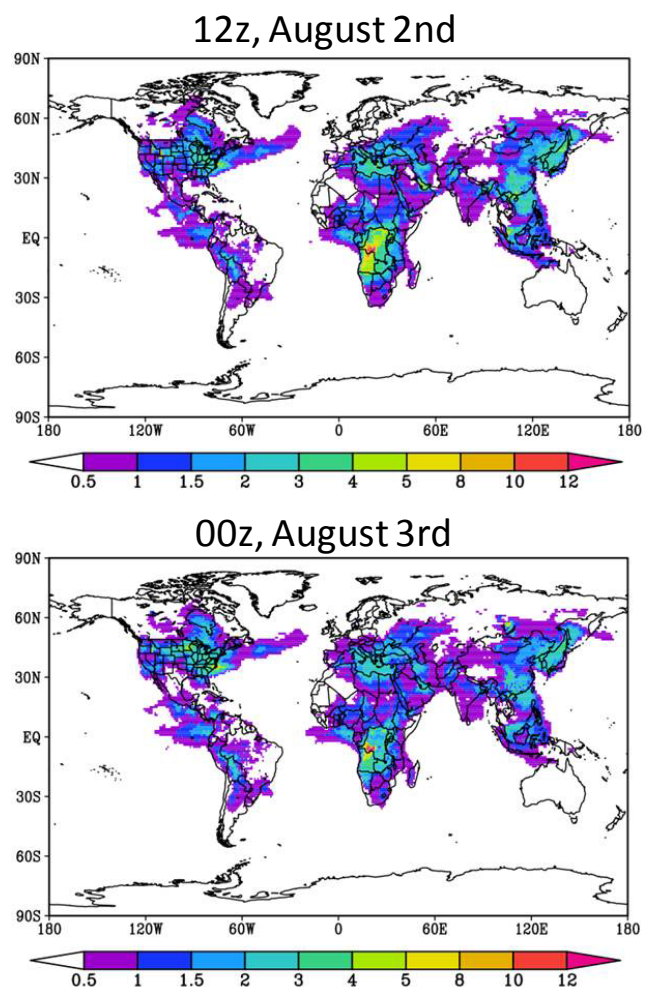
Figure 5: 120 hours forecast of surface SOA using RACM_SOA_VBS scheme at 12z August 2nd and 00z August 3rd 2016.
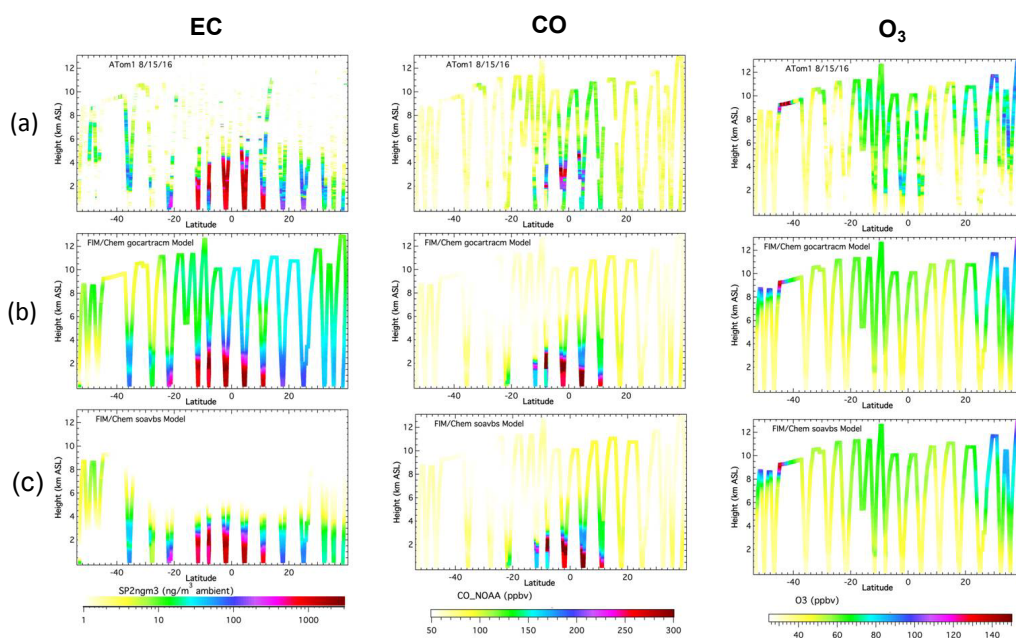
Figure 6: Height-latitude profiles of EC, CO and O3 over Atlantic on August 15th and August 17th, 2016 for (a) ATom-1; (b) RACM_GOCART; and (c) RACM_SOA_VBS.
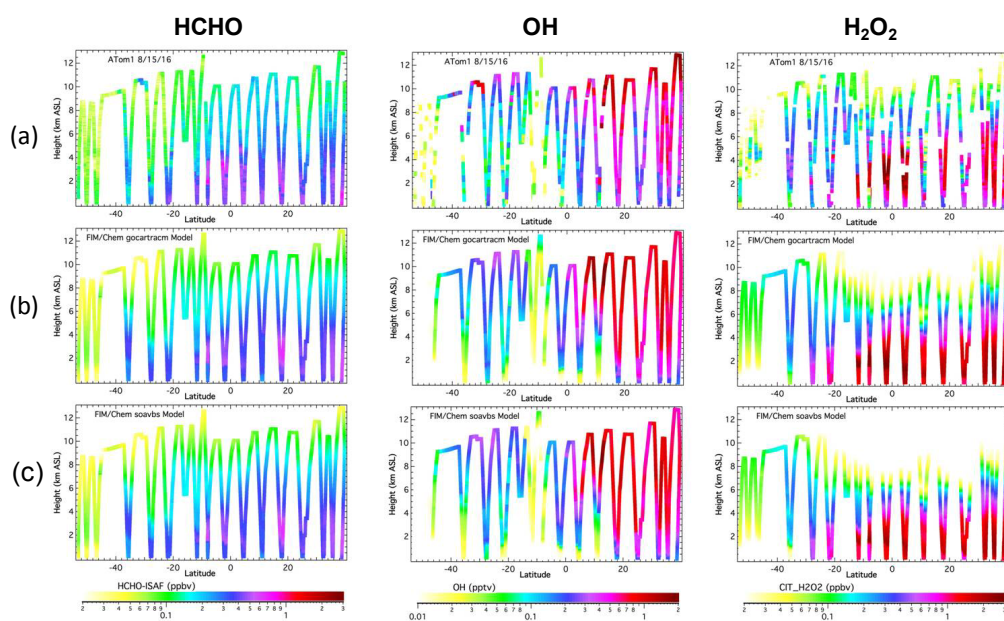
Figure 7: Height-latitude profiles of HCHO, OH and H2O2 over Atlantic on August 15th and August 17th, 2016 for (a) ATom-1 observations; (b) RACM_GOCART; and (c) RACM_SOA_VBS.
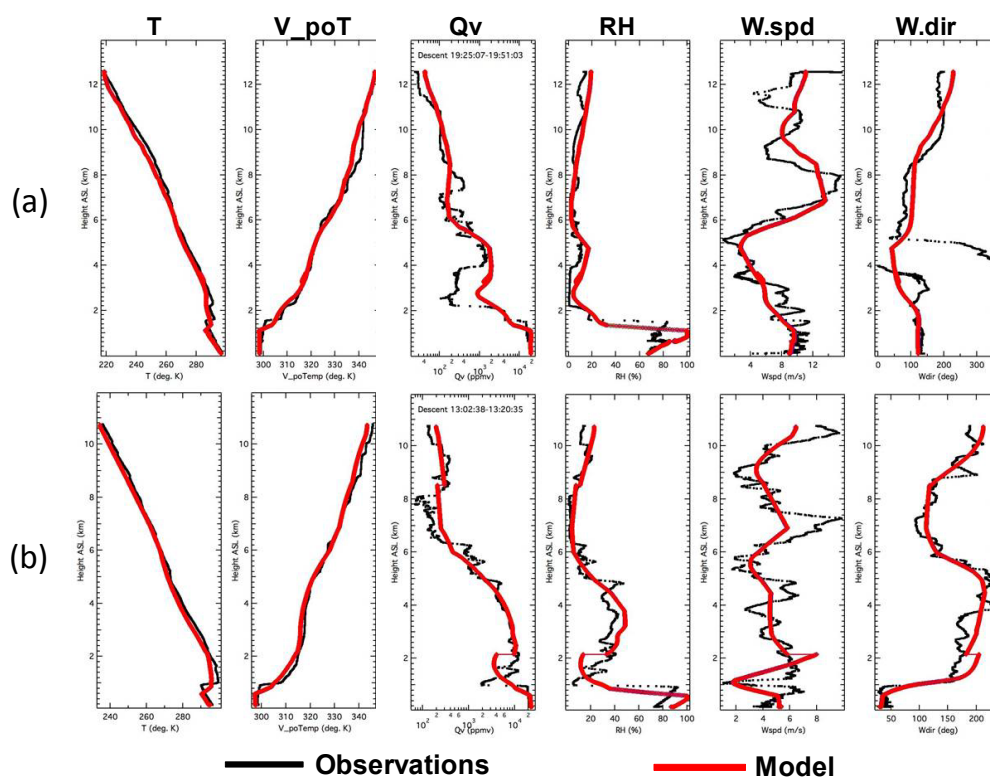
Figure 8: ATom-1 observations and model results for temperature, virtual potential temperature, water vapor, relative humidity, wind speed and wind direction in the (a) biomass burning and (b) dust events. The biomass burning plume is from August 15, 2016, profile #16 near 20?S while the Saharan dust plume is from August 17, 2016, profile #10 near 25?N.
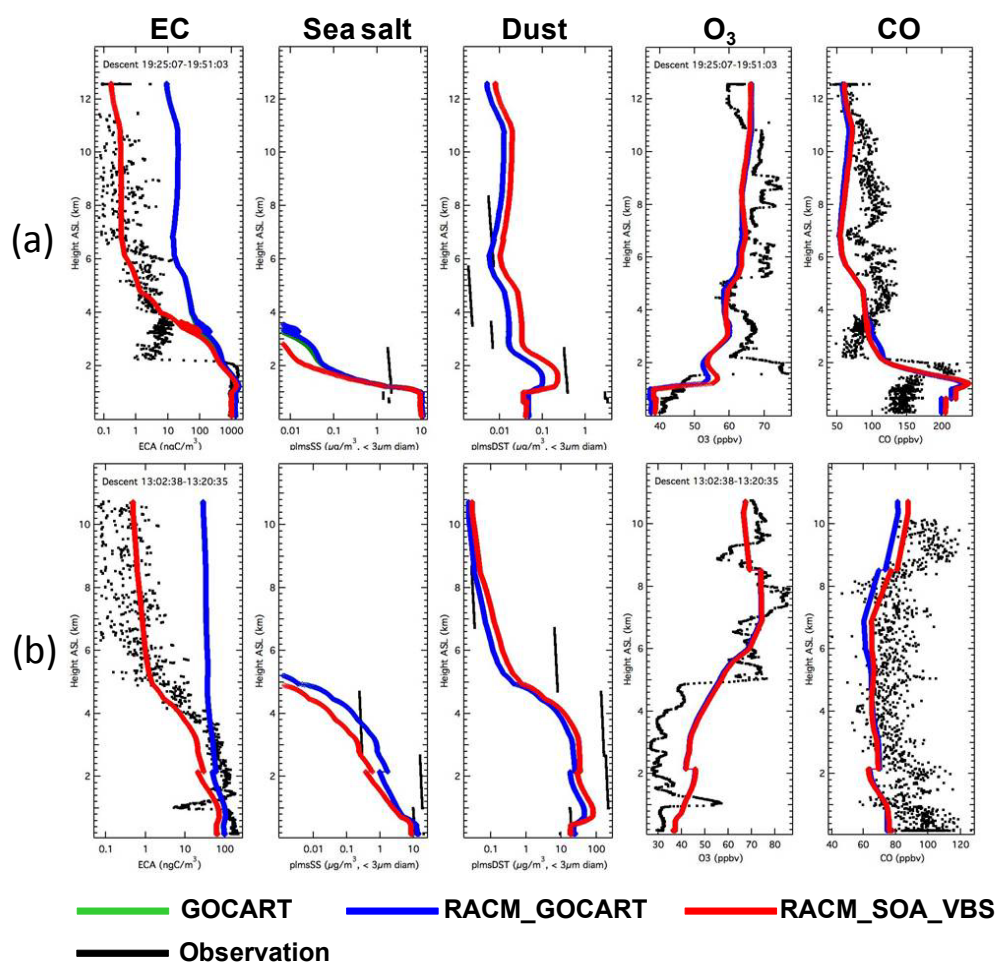
Figure 9: Comparisons between ATom-1 observations and model vertical profiles of EC, sea salt, dust, O3 and CO in the biomass burning (a) and dust (b) events. The biomass burning plume is from August 15, 2016, profile #16 near 20?S while the Saharan dust plume is from August 17, 2016, profile #10 near 25?N. Green and blue lines are nearly identical for aerosol.
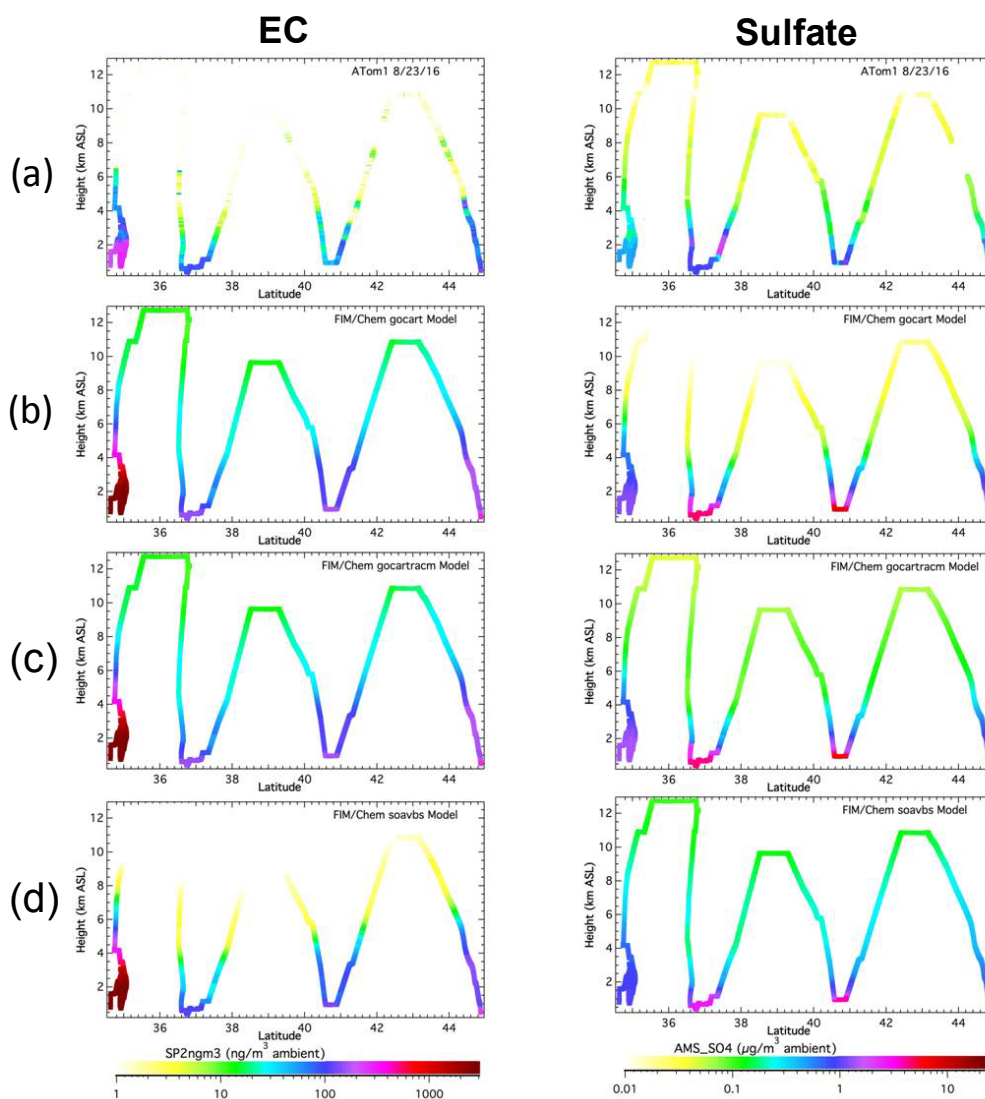
Figure 10: Height-latitude profiles of EC and sulfate over United States on August 23rd, 2016 for
(a) ATom-1; (b) GOCART; (c) RACM_GOCART; and (d) RACM_SOA_VBS.
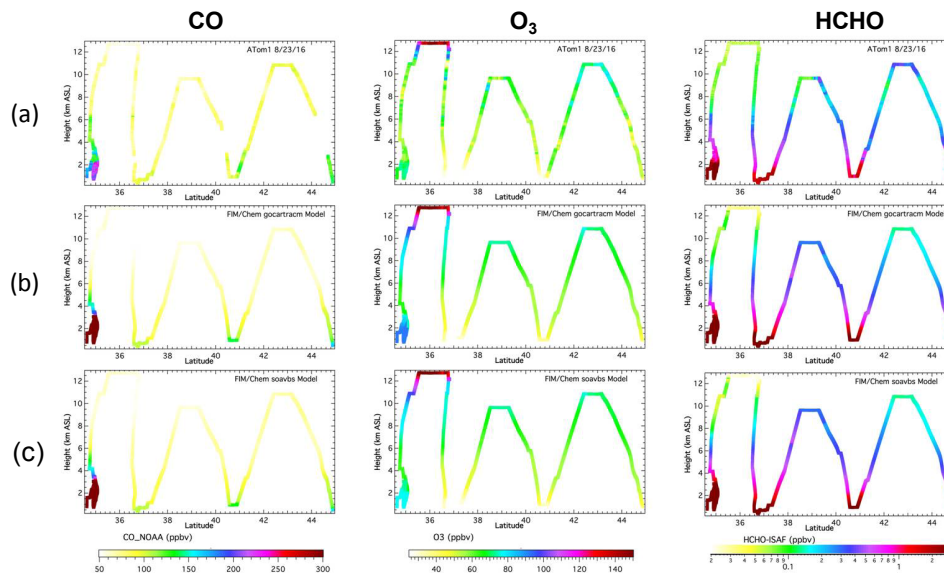
Figure 11: Height-latitude profiles of CO, O3 and HCHO over United States on August 23rd, 2016 for (a) ATom-1; (b) RACM_GOCART; and (c) RACM_SOA_VBS.
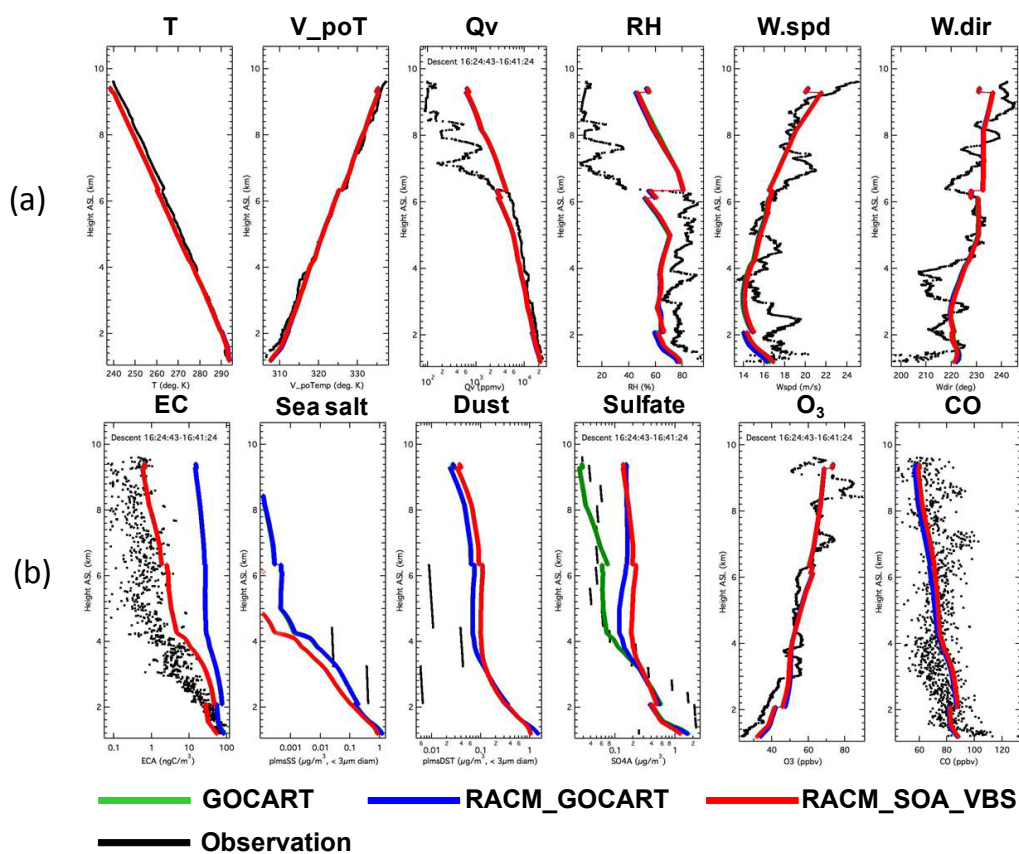
Figure 12: Observations and model results for profile #4, 8/23/16 over southeastern Kansas.
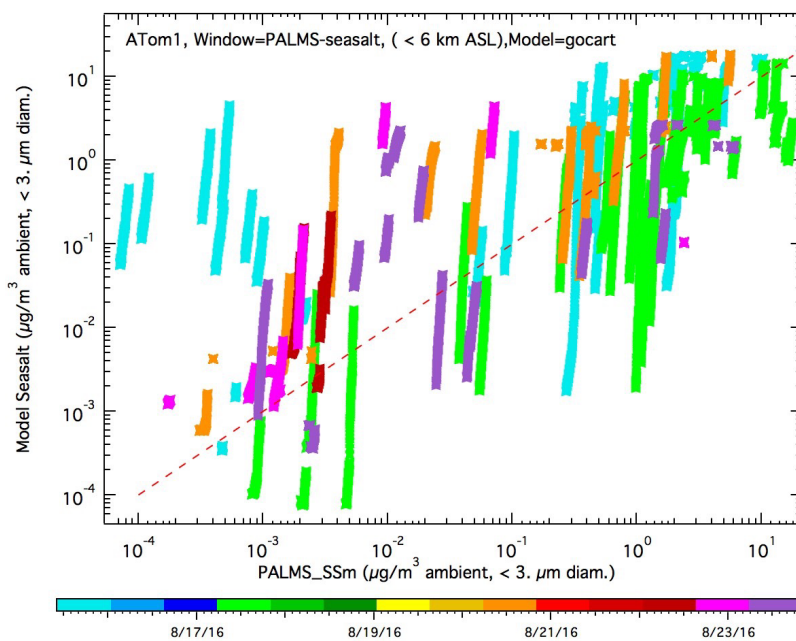
Figure 13: GOCART model forecast versus ATom-1 observed sea salt below 6 km.
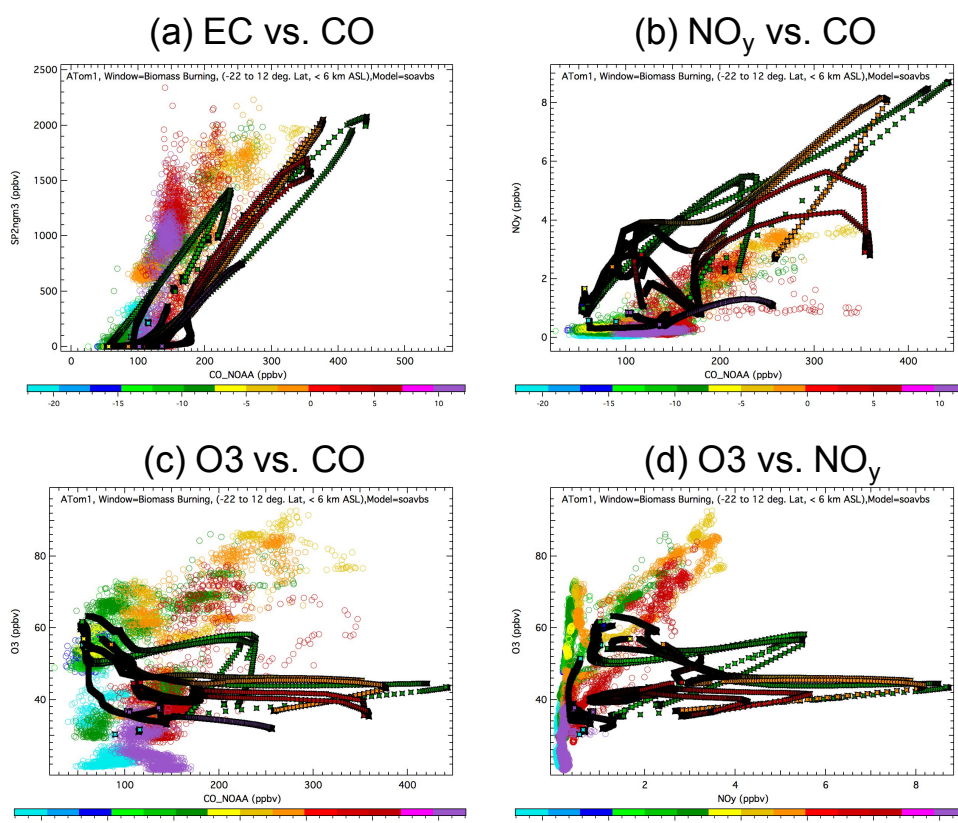
Figure 14: Model (black color dot) and observation (color dot) ratios of (a) EC relative to CO; (b) NOy relative to CO; (c) O3 relative to CO and (d) O3 relative to NOy. Color scale is degree latitude.